

Figure. 9. Plots of the concentrations of Min proteins: (a) MinD and (b) MinE. The plots are focused at the left end grid (·), and the right end grid (x) as functions of time in seconds for J = 0.0 m/s to J = 0.3 m/s. The vertical scales denote numbers of protein copies in the system. The horizontal scale spans time for 500 s.

Dear Editors,

Please find attached the MS word file of our manuscript for reviewing. It is to submit to BioSystems. The manuscript details are as follows.

Title: Stochastic modeling of the effect of an external electric field on the Min protein Dynamics in E. coli

Keywords: Electric fields, E. coli, Cell division, Min proteins, MinCDE oscillation, stochastic process

Authors: Charin MODCHANG, Wannapong TRIAMPO*, Paisan KANGTHANG, Udorn JUNTHORN, Somrit UNAI, Waipot NGAMSAAD, Narin NUTTAWUT, Yongwimon Lenbury

Address: Department of Physics, Faculty of Science, Mahidol University, Rama 6 Rd.,

Ratchatewee,

Bangkok 10400, Thailand Telephone: 664-004-2689

Fax: 662-201-5843

E-mail: wtriampo@yahoo.com and scwtr@mahidol.ac.th

Thank you so much for your concern in advance and with all my best regards. Anything else we can do for this matter please feel free to let me know.

Sincerely yours,

Wannapong Triampo

Response of pathogenic spirochete *Leptospira interrogans* serovar Canicola to ultaviolet-A irradiation

Jirasak Wong-ekkabut^a, Wannapong Triampo^{a,f,g}*, Duangkamon Baowan^c, Sudarat Chadsuthi^a, Galayanee Doungchawee^b, Chartchai Krittanai^e and I Ming Tang^{a,d,f}

^aR&D Group of Biological and Environmental physics, Department of Physics, ^bDepartment of Pathobiology, ^cDepartment of Mathematics, ^dCapability Building Unit in Nanoscience and Nanotechnology, Faculty of Science, Mahidol University, 272 Rama VI Road, Ratchathewi, Bangkok 10400, Thailand ^cInstitute of Molecular Biology and Genetics, ^fInstitute of Science and Technology for

^eInstitute of Molecular Biology and Genetics, ^fInstitute of Science and Technology for Research and Development, ^gCenter for Vectors and Vector-Borne Diseases (CVVD)Mahidol University, Nakhonpathom 73170, Thailand

15 Received

5

10

25

30

35

40

*To whom correspondence should be addressed:

Phone: +662-201-5853; Fax: +662-201-5843

E-mail: scwtr@mahidol.ac.th

20 Abstract:

The effect of exposure of ultaviolet-A (UVA) radiation was studied on the pathogenic spirochetes Leptospira interrogans serovar Canicola for different time durations. The changes in cell growth and viability due to the UVA exposure were determined by using conventional microscopic agglutination test (MAT), dark-field microscopy and spectrophotometry measurements. Changes in antigens and protein expression in the cells were detected by sodium dodecylsulfate polyacrylamide gel electrophoresis (SDS-PAGE) and immunoblot. The decrease in cell growth and viability were found to be exposure period or dose dependent. The growth decreased sharply with very high rate for the first 24 h of exposure, then the growth reached the minimum within about 1d exposure period and level-off for the further treatment until 7d exposure period. Immunoblot revealed the presence of 21 kDa antigenic protein in the unexposed cells, which disappeared after exposure to UVA of 24 h. SDS-PAGE analysis indicated the presence of the 76 kDa protein band in the cells exposed to UVA for 2 h to 24h. For more than 2h to 24h exposure to UVA decreased this protein, but the proteins of molecular mass between 56 kDa and 70 kDa appeared. This work is the first step toward the understanding of the effects of UVA on leptospira bacteria. With further investigations especially about mechanisms of how UVA interact with leptospira, it will eventually lead to development of new strategies to control or prevent leptospira in the environment.

Keywords: Ultraviolet-A, Leptospirosis, *Leptospira interrogans* serovar Canicola, Immunoblotting, SDS-PAGE

Leptospirosis, a zoonotic disease caused by the pathogenic spirochetes, belonging to the family *Leptospiraceae*, genus *Leptospira* has become a public health problem throughout the world. More than 250 serovars of this bacterium have been reported, based on microscopic agglutination test (MAT). The problem is more severe in humid tropical and subtropical countries such as Thailand¹, Nicaragua² and India³, than the countries having a temperate climate. The incidence of disease ranges from approx 10-100 per 100,000 to 0.1-1 per 100,000 per year in humid tropics and temperate climates⁴. The disease is transmitted via indirect contact with contaminated water and soil⁵ or direct exposure to infected animals and their products^{6,7}, mainly urine. Both wild and domestic animals, such as rodents, heifers, and canines are the natural hosts.

Typically, *Leptospira* are aerobic and motile spirochetes with helical or spiral structure and a unique (among the spirochetes) hook at both ends (Fig. 1). They are about 0.1-0.2 μm wide and 6-20 μm long and having helical amplitude of approx 0.1-0.15 μm and wave length about 0.5 μm^{8,9}. Their ultra-structure comprises a double cytoplasmic membrane, in close contact with a peptidoglycan layer and an outer membrane¹⁰. The composition of lipopolysaccharide (LPS) of their outer membrane is similar to other gram-negative bacteria¹¹, but has a lower endotoxic activity¹². Optimal conditions for the growth of this organism is well documented^{8,13}. The most suitable conditions for their survival outside the host are a moist environment with a neutral pH and a temperature range between 20-32°C.

Leptospira are highly susceptible to adverse environments such as dry atmosphere, chemicals (chlorine or iodine in detergents), unfavorable pH (>8.0 or <6.5), magnetic fields¹⁴, and high temperatures (above 40°C). High-energy ultraviolet irradiation (UVC) is effective in destroying the leptospira and other microorganisms^{15,16}. Earlier, effects of UVA have been studied on eukaryotic cells, animal tissues, prokaryotic cells such as E. coli¹⁷ as well as other bacilli or coci bacteria¹⁸. However, results in other bacteria may not be able to be used to explain the case of spirochetes, due to differences in their morphological characteristics, motility, and virulence-related structure. In addition, there are also differences at genomic and proteinomic levels. For instance, Leptospira has two circular chromosomes, in contrast to linear chromosomes and chromatids in Berrela. Also, unusual features are found in their ribosomal gene organizations. In Leptospira, within the genomic decoding, enormous diversity has been found in the genetic organization of different serovars. Thus, spirochetes could be considered a unique group in microbial world.

In the present study, the effects of UVA stress on the growth and activity of L. interrogans serovar Canicola have been studied. Cell growth and viability have been determined by conventional microscopic agglutination test (MAT), dark-field microscopy, and spectrophotometry. Changes in antigens and protein expression in the cells have been determined by SDS-PAGE and immunoblot. The work is aimed to gain the better understanding of the response of leptospira under the stress of UVA irradiation, in order to develop effective strategies to limit their survival in natural environment by introducing UVA light source or adapting the risk area to be more exposed to sunlight. With this regard, various water treatment technologies including direct photolysis and bacterial inactivation by inherently produced free radical by UVA could be improved greatly and economically.

Materials and Methods

5 Strain and culture conditions of leptospira

Pathogenic *Leptospira interrogans* serovar Canicola were obtained from the National Leptospirosis Reference Center, National Institute of Health (NIH), Thailand and grown in the Ellinghausen and McCullough liquid medium as modified by Johnson and Harris (EMJH)^{8,19} at about 27°C. The samples were sub-cultured on a weekly interval. Each of 3 ml bacterial culture in 1.5 cm diameter glass tube had an initial optical density (OD) at 400 nm of about 0.10, as measured by a UV-VIS spectrophotometer. This was equivalent to 1+ level as graded using a dark-field microscope which in turn indicated a cell concentration of ~10⁸ cells/ml.

15 UVA irradiation source

10

20

30

35

40

45

50

The UVA radiation was generated by a 20 W T12 fluorescent lamp, Backlight (Sylvania Co.). The lamp produced a continuous emission spectrum (320-400 nm) and a peak at 365 nm, measured by HR2000CG-UV-NIR high-resolution composite-grating Spectrometer (Ocean Optics, Inc.). The UVB and UVC radiations were absorbed by the glass tube. The experimental leptospira samples were exposed to UVA radiation of intensity of about 1.3 mW/cm², as measured by a 1830-C optical power meter with detector and calibration module model 818-UV/CM (Newport Corporation.).

25 Irradiation procedure

Separate leptospira samples were exposed to UVA at a distance 20 cm from the source of radiation for 0, 5, 15, 30, 45, 60, 120, 180 and 360 min on day 1, and for several more days (1 to 7 days). After exposure, all cultured samples were maintained for a further 7 days. On 7th day post-treatment, all the samples were taken for measurements of their viability and growth using a dark-field microscope (Axiloab Pol 2, Carl Zeizz Co.) mounted with a CCD camera. Micrographs were taken using the AxioVision AC 4.1 software. Semi-quantitative techniques based on microscopic agglutination test (MAT), turbidity-based method, UV-VIS spectrometer were also employed. Protein or antigenic changes were determined by using SDS-PAGE. Experiments were repeated at three times under the same conditions with separated occasions.

Growth and cell survival

The techniques mentioned above were used to monitor the bacterial growth and survival.

Qualitative analysis by dark-field microscopy

The growth and survival of treated leptospira were determined by looking at cell density, mobility²⁰ and morphology. Since due to their very thin size and poor uptake of conventional dyes, leptospira could not be observed by ordinary light microscope, dark-field microscopy (DFM) was used⁴. In DFM, an oblique light beam was cast on to the leptospira (lying on a microscope slide) using a special condenser, when the central illuminating light beam was interrupted. The leptospira could then be seen as silvery threads in a dark background. To assess the effect of UVA on the growth and survival, samples were diluted 10-fold on 7th day post-treatment and were observed with a dark-field microscope.

Semi-quantitative analysis by microscopic agglutination test (MAT)

MAT is a standard serological technique used in the diagnosis of leptospirosis⁴. It is used in combination with the enzyme-linked immunosorbent assay (ELISA). It is a reference test and is used to detect the presence of the antibodies and determine their titer. It can also be used to determine relative growth of bacteria colony. The method is simple and consists of mixing the test serum with a culture of leptospira and then evaluating degree of agglutination using a dark-field microscope.

The reference-specific antiserum against L. interogans serovar Canicola was required for the test. Leptospira samples were mixed with 2-fold dilutions of antiserum (1:100, 1:200, 1:400, 1:800, 1:1600, 1:3200, 1:6400) and incubated for 2 h at room temperature. The agglutination reactions were then observed under a 200x dark-field microscope and scored as follows: 4+, 3+, 2+, 1+ = 100%, 75%, 50%, 25% absence of free leptospira from the field, respectively.

15

20

25

30

35

40

45

50

5

10

Quantitative analysis by UV-VIS spectroscopy

An UV-VIS spectrometer (V-530 UV/VIS spectrometer, Jasco Internationl Co., Ltd.) was used to quantify the amount of *Leptospira* present by light absorption measurement in the UV-VIS spectrum^{8,21,22}. These were done on exposed leptospira cells (for different exposure times) taken on the 7th day of their cultivation. Solutions of the leptospira cells were placed into cuvettes made with quartz SUPRASIL (200-2500 nm) with light path 10 mm (type no. 100.600-QG, Hellma Co.). A single beam spectrometer operating in the range of 200-800 nm was used. The OD or absorbency at 400 nm was taken²¹. All samples were obtained with already used EMJH liquid medium as the blank.

Scanning electron microscopy (SEM)

Samples were washed three times with normal saline (0.9% NaCl) at $10,000 \times g$ for 10 min and dropped on poly-L-lysine-coated cover glass slide for 1 h. Samples were prefixed directly with 2.5% glutaraldehyde for 2 h at room temperature and then washed three times with 0.01 M phosphate buffer (pH 7.3) for 10 min. All samples were post-fixed with 0.1% osmium tetroxide. After fixation, samples were dehydrated with increasing concentrations of ethanol, critical point-dried (HPC-2 critical point dryer, Hitachi), and coated with platinum-palladium ion sputter (E102 ion sputter, Hitachi) for 2 min. The micrographs were taken with accelerating voltage of 15 kV SEM (S2500, Hitachi) on the negative film.

SDS-PAGE and immunoblot

Whole cell solublization

Leptospiral cultures were centrifuged at $10,000 \times g$ for 10 min and the pellets were washed three times in normal saline (0.9% NaCl) and then solublized in SDS-PAGE sample buffer composed of 0.35 M Tris.Cl (pH 6.8), 10% SDS, 30% glycerol, 9.3% dithiothreitol (DTT) and 0.175 mM bromophenol blue²³.

Gel electrophoresis and immunoblot

For one-dimensional SDS-PAGE, other samples were solubilized in SDS-PAGE sample buffer. The samples were heated at 100°C for 10 min²³. The 3 µl of each sample was loaded on to 12% polyacrylamide gels²⁴ and electrophoresed at 200 voltages for 55 min. The molecular mass protein standards (Amersham) used were: rabbit muscle phosphorylase B (97 kDa), bovine serum albumin (66 kDa), hen egg-white ovalbumin (45 kDa), bovine carbonic anhydrase (31 kDa), soybean trypsin inhibitor (20 kDa), and hen egg-white lysozyme (14 kDa). After electrophoresis, gel

was separated into two parts. One part was stained with Coomasie brilliant blue (0.025% Coomassie R-250, 40% methanol, 7% acetic acid) for 1 h and then destained with destaining solution I (40% methanol, 7% acetic acid) for 1 h and fixed with destaining solution II (5% methanol, 7% acetic acid). The other part was blotted on to a polyvinylidene difluoride (PVDF) membrane at 1.6 mA/cm² for 70 min. After transfer, membranes was incubated with 0.1%(w/v) Ponceau S in 5% (v/v) acetic acid (Merck) and washed with 2% skimmed milk and 0.2% tween20 (Sigma, USA) in phosphate buffer saline (PBS).

For immunological detection, the membrane was incubated with primary antibody (rabbit reference antiserum specific to *L. interrogans* serovar Canicola) at 1:1,000 dilutions in 2% skimmed milk and 0.2% tween20 in PBS for 1 h, and washed three times for 10 min each in 2% skim milk and 0.2 % tween20 in PBS. Thereafter, the membrane was transferred to a solution of secondary antibody [polyclonal goat anti-rabbit immunoglobulin HPR (DakoCytomation P0448)] at 1: 2,000 in 2% skimmed milk and 0.2% tween20 in PBS, incubated for 1 h, and then washed three times for 5 min each in PBS. Color was developed with a solution of 1.25 mg of diaminobenzidine (DAB) and 5 μ l of 35% H₂O₂ in 10 ml of PBS. The membrane was then rinsed in several changes of PBS to stop the reaction, air-dried and photographed. **Results**

UVA effects on growth and survival of L. interrogans

The growth curve of *L. interrogans* serovar Canicola is given as a plot of the number of leptospira (proportional to the measured OD values) present at a particular time. This growth could be well-fitted to a Gompertz function²⁵ ($y = ae^{-\exp{-k(t-t_c)}}$) with parameters $a = 0.43 \pm 0.02$, $k = 0.75 \pm 0.13$, and $t_c = 0.62 \pm 0.15$. The OD value, which was proportional to cell number density increased exponentially to 400% (OD = 0.40) of initial value after 3 days of cultivation and then approached a steady state (OD of about 0.45 times of its initial value) until the day 7 (last day of observation) as seen in figure 2. This figure 2 shows the Gompertz-like growth, which might be due to the food limitation and increased cell toxicity, due to over-crowding of population. The presence of intermediate region in Gompertz curve indicated that in nature, bacterial life alternates between growth and stationary phases, primarily due to the fluctuations in nutrient availability.

To see the effects of UVA irradiation exposure on *L. interrogans* serovar Canicola, all samples (control and treated) were cultivated for the same length of time (7 days). To gain a visual impression of what was occurring, the growth of the leptospira samples exposed to UVA radiation for 0, 30, and 360 min and for 1 to 5 days was monitored using a dark-field microscope. Fig. 3a shows the dark-field images of samples cultivated for 7 days. The images clearly showed a decrease in the number of bacteria present, as the exposure duration increased. The mobility of cells appeared to decrease as the exposure time increased. Some untypical morphology was observed after a 1-day exposure. We used an atomic force microscopy (AFM), operating in the tapping mode to obtain images of the control cell and that exposed to the UVA for 1-day. Fig. 3b shows that the spiral period had become longer. The SEM micrograph also exhibited the same trend as observed in Fig. 3c. However, the mechanism by which the leptospira morphology changes, is still unknown.

The OD of the leptospira exposed to the UVA for various time durations is shown in Fig. 4. Results showed a decrease of OD, as the exposure time increased up to 1 day and after 1-day exposure, OD did not change significantly. Theses results were consistent with those obtained with conventional MAT measurements (Table 1). The agglutination reactivities of bacteria exhibited a relative decrease with increase in

exposure time. The changes in the agglutination reactivities became very small after an exposure to UVA of more than 1 day. Fig. 5 shows the dark-field micrographs of agglutination of leptospira after reacting with the specific antiserum (at dilution 1:100). It showed small changes in the agglutinating size and in the features of the exposed samples (Fig. 5B) from those of control cell (Fig. 5A). A change in agglutination pattern was observed only after the samples were exposed to the UVA radiation for at least 1 day.

The change in the formation pattern could possibly be due to the low leptospira concentration or denaturing effect of the antigen-antibody reaction. Therefore, we compared agglutination reactivities of low concentration of unexposed leptospira sample and sample exposed for 1-day that had produced the same OD and found two patterns more or less qualitatively similar (data not shown). Thus, it was concluded that the changes in agglutination reactivities and reactivity patterns were due to the use of low concentrations of cells.

Finally, to test the hypothesis that results for the effects of UVA irradiation up to 24 h (112.3 J/cm²) may mainly cause temporarily injured or dead cells due to the UVA treatment. We then perform the post treatment effect or long-term effect study. To do so, we re-subcultured the unexposed and exposed samples and monitored their growth in the dark. After 7 days of culture, the samples exposed to UVA for 24 h or more did not normally grow i.e., the pre-exposed cells were more or less dead (data not shown). Otherwise, these cells would re-grow if they were just temporary injured or inactive. Whereas the cells exposed for lesser than 24h could grow but their growth is not as good as control one. These results may be implied that after the treatments, cells were injured when exposed less than 24 h and become more injured and/or killed after 24 h or more UVA exposure.

UVA effects on protein and antigenic components

SDS-PAGE and immunoblot test were used to investigate UVA-induced antigenic denaturation. Electroseparated protein components were visualized on the gel by Coomasie blue staining or transferred to PVDF membrane and immunostained with reference antiserum, specific to Canicola. The results of immunoblot of the unexposed (control) sample and UVA-exposed samples at 2, 6 and 24 h are shown in Fig. 6. Sample exposed to 24 h (lane 4) showed the absence of antigen with molecular mass of about 21 kDa, whereas this band was observed in control (lane 1), 2 h (lane 2) and 6 h (lane 3) exposed samples.

Fig. 7 shows SDS-PAGE analysis of the proteins in leptospira cells exposed to UVA radiation for 2, 6 and 24 h. Compared to control (lane 4), 24 h exposure (lane 3) a 76 kDa protein band appeared. The 76 kDa band which appeared after a 2 h-exposure begins to disappear as longer radiation times are used (compare lane 1 with lanes 2 and 3). Proteins having molecular masses between 56 kDa and 70 kDa also appeared in lanes 2 and 3, possibly due to the degradation of 76 kDa protein, induced after 2 h of exposure to UVA.

Discussion

5

10

15

20

25

30

35

40

45

50

For the results of less than 24h UVA exposure, they demonstrated that UVA could temporally cause the cell damages or injures as a consequence of inhibiting the growth of leptospira. Hence, it allows the growth recovery and subsequently regrowth of bacteria after UVA is removed. This thought was confirmed by the results of post-treatment or long-term effects study. In contrast, when the exposure time was longer (from 24 h up-to 7d), the permanent inactivation or bactericidal effect was

consistently observed as once again can be confirmed by post-treatment studies. Therefore, these findings indicate the UVA effects are dose-dependent. Regarding to this information, our experimental set-up design may correspond to the daily doses in the real world environment as follows. The UVA doses used here are consistent with those used in ref. 26. There, Maneewan and co-workers²⁶ measured the average daily intensity of solar radiation in Thailand to be about 17.5 MJ m⁻² day⁻¹ or 20.3 mW/cm². However, the UVA only accounts for about 5% of solar intensity or is equivalent to 1.03 mW/cm². Hence in terms of doses used it may be reasonable to say that our experimental design is practical. However, there are other factors that may play roles in these effects such as the depth of the water reservoir, the flow and the aeration rate of water, etc. Therefore, more works need to be done to make connection between our findings and the possible future implementation of the leptospirosis control.

Considering change in morphology of UVA exposed leptospira comparing with unexposed leptospira, the unusual thinner in size and less spiral in shape were remarkably observed. The possible explanations may concerns the structure of the leptospira affected by UVA irradiation. This was very pronounced for the treatment of 24 h exposure (Fig. 3b and c). It is known that Axial filament is the skeleton of the spiral structure 27,28. Hence, it is reasonable to say that the changes in the morphology due to UVA exposure might involve this structure. Specifically, the axial filament is responsible for the locomotion of leptospira 2,8,29, the damage to it thus could cause the leptospira to become less active and less mobile (observed under dark field OM observation). Previously, Silva and co-workers reported about the loss of helical shape due to damage of axial filament. They demonstrated that the abnormal of spiral shape of leptospira could be subjected to pressure. Moreover, they also suggested that the leptospira could become less mobile as a result of morphological changes. These findings appeared to support our results.

Now, we turn into the UVA effects on leptospira at molecular level. It is known that UVA radiations induce cellular and molecular changes such as damage to DNA, proteins and lipids in human and bacterial cells³⁰⁻³². They can induce the formation of reactive oxygen species (ROS) in the cells³³⁻³⁵, which may cause photooxidation of membrane-bound content and damage the cell membrane and DNA^{36,37}. This may result in the lowering of growth and associated denaturation of morphology. As spirochetes including *Leptospira interrogans* have shown differences in cell membrane and axial filament from other bacteria, further studies on UVA exposure on are required to gain insight into mechanisms of this specific system.

One of the interesting observations in SDS-PAGE analysis was the appearance or induction of the 76 kDa protein (not found in control or unexposed cells) in *L. interrogens* serovar Canicola, after exposure to the UVA radiation for 2 h. Nally and co-workers³⁸, reported that *L. interrogans* serovar Pomona could respond to the external stress by synthesizing the proteins or other cellular constituents, necessary for its survival in a changed environment including temperature and pH. These findings may suggest that *L. interrogans* could response to the perturbed stress including UVA stimuli by such as expressing proteins. Guerreiro and co-workers studied on the leptospiral proteins recognized during the humoral immune response to leptospirosis in humans focusing on *L. interrogans* serovar Copenhageni³⁹. They reported that two major antigens p62 and p76 identified as chaperones GroEL and DnaK respectively, were found in these bacteria in the 2-D immonoblot of the proteins, when probed with pooled convalescent-phase sera from leptospirosis patients. The p76 protein (band under 82 kDa) is a bacterial heat-shock protein and is upregulated by elevated temperatures. It was identified as the target of the humoral response during natural

infection and plays an important role in the repair, folding and assembly of proteins following heat stress⁴⁰. *L. interrogans* serovar Hardjo could also rapidly synthesize the p62 and p76 proteins, as a consequence of a sudden increase in the temperature⁴¹.

From our results, SDS-PAGE analysis showed the intensity of the 76 kDa band of 2 h exposed cells was very noticeable when compared with those of 6 h or longer exposed samples. To understand these results, it may be useful to relate these with the growth. From the growth curves, it was seen that compared with 2 h or longer exposed samples, those for 2h exposed group has much greater number of leptospira including those were active and alive. Those active leptospira are the ones that believed to be able to express the stress-response proteins. Concerning our electrophoresis results, this interesting phenomenon may suggest that only active cells express 76 kDa proteins for responding to the environment stress. Hence, it was why the 76 kDa proteins appearance became fader as the exposure times (6h or higher) were longer. From, these findings, it might suggest that if we want to treat or get rid of leptospira, the dose to be used must be large enough. Otherwise, leptospira may just temporarily inactive or somehow induce the defense mechanism or response to the treatment.

Another interesting finding was the disappearance of 21 kDa protein band in the immunoblot of *L. interrogans* of 24 h exposed cells to the UVA radiation. This result may indicate denaturation of this antigenic component at a high dosage of UVA. Previously, Cullen and coworkers^{42,43} studied *L. interrogans* serovar Lai and reported that a 21 kDa protein (lipL21) was found to be the second major constituent of the outer membrane proteome. It was also found later that LipL21 is expressed during infection and conserved in the pathogenic *Leptospira* species, whereas it was not be detected in nonpathogenic *Leptospira biflexa*⁴⁴. Therefore, these evidences seems indicated that the degradation of 21 kDa band due to UVA might reduce virulence of *Leptospira interrogans* which are pathogenic leptospira. However, to be able to draw any conclusion about the present study in terms of the correlation between 21 kDa band for UVA exposed sample and leptospira virulence, more works are needed to be done.

The above statements may support the fact that why leptospirosis mainly occur in the rainy season. Because of the water-borne bacterial nature of leptospira and possibly the lesser UVA radiation exposure period during the rainy season, these may result in the optimal condition for the growth of leptospira. Of course, water and tropical climate like environmental condition certainly are the major factors of the growth and spreading of these leptospira, UVA from sun light could more or less contribute to the spread of leptospirosis. However it also should be mentioned that based on this study, one may take advantage of UVA radiation as a bactericidal or bacteriostatic factor to further development of new strategies to control leptospira in the environment. For example, one could adapt or set the landscape of household as well as the environments where are susceptible or very high risk areas to be more exposed to UVA radiation. Or combination of UVA radiation and other photocatalytic materials like titanium dioxide (TiO₂) may be other alternatives ^{45,46}.

Acknowledgement

We thank Dr. Toemsak Srikirin for providing UVA detector, Suchada Geawduanglek, Pranom Puchadapirom and Suraphol Kongtim for technical assistance, and members in Biophysics group (Harit Pitakjakpipop, Titiwat Sungkaworn), Department of Physics, Faculty of science, Mahidol University for their

helpfulness. This research work was financially supported in part by Mahidol University (MU), The Thailand Research Fund (TRF), National Center for Engineering and Biotechnology, Thailand (BIOTEC) and The Academy of Sciences for the Developing World (TWAS) to W Triampo. The support of the Royal Golden Lubilea Ph. D. Program (PHD/0240/2545) to L Wong akkebut and L Ming Tang is also

Jubilee Ph.D. Program (PHD/0240/2545) to J Wong-ekkabut and I-Ming Tang is also acknowledged.

References

15

30

45

- 1. Watt G, Jongsakul K & Suttinont C (2003) Am J Trop Med Hyg 68, 89-91
- 10 2. Brandling-Bennett A D & Pinheiro F (1996) Emerg Infect Dis 2, 59–61
 - 3. World Health Organization (2000) Leptospirosis, India: Report of the investigation of a post-cyclone outbreak in Orissa, Wkly Epidemiol Rec WHO, Nov. 1999, pp. 217–223
 - 4. World Health Organization (2003) *Human leptospirosis*: Guidance for diagnosis, surveillance and control
 - 5. Levett P N (2001) Clin Microbiol Rev 14, 296–326
 - 6. Tangkanakul W, Tharmaphornpil P, Plikaytis B D, Bragg S, Poonsuksombat D, Choomkasien P, Kingnate D & Ashford D A (2000) *Am J Trop Med Hyg* 63, 204–208
- 7. Douglin C P, Jordan C, Rock R, Hurley A & Levett P N (1997) *Emerg Infect Dis* 3, 78–80
 - 8. Faine S, Adler B, Bolin C & Perolat P (1999) *Leptospira and Leptospirosis*, 2nd edn, MediSci Ed, Melbourne Australia
 - 9. Goldstein S F & Charon N W (1990) Proc Natl Acad Sci (USA) 87, 4895-4899
- 25 10. Haake D A (2000) Microbiology 146, 1491–1504
 - 11. Vinh T, Adler B & Faine S (1986) J Gen Microbiol 132, 103-109
 - 12. Shimizu T, Matsusaka E, Takayanagi K, Masuzawa T, Iwamoto Y, Morita T, Mifuchi I & Yanagihara Y (1987) *Microbiol Immunol* 31, 727–735
 - 13. Faine S (1982) *Guideline for control of leptospirosis*, Vol. 67, pp. 129, World Health Organization, Geneva
 - 14. Triampo W, Doungchawee G, Triampo D, Wong-ekkabut J & Tang I M (2004) *J Biosci Bioeng* 98, 182–186
 - 15. Srikanth B (1995) The Basic Benefits of Ultraviolet Technology, Water Conditioning & Purification
- 35 16. Stamm L V & Charon N W (1988) Appl Environ Microb 54, 728-733
 - 17. Pizarro R A (1995) Int J Radiat Biol 68, 293-299
 - 18. Taber H, Pomerantz B J & Halfenger G M (1978) *Photochem Photobiol* 28,191–196
 - 19. Ellinghausen H C & McCollough W G (1965) Am J Vet Res 26, 45-51
- 40 20. Silva C C M, Giongo V, Simpson A J G, Camargos E R d S, Silva J L & Koury M C (2001) *Vaccine* 19, 1511–1514
 - 21. Tchamedeu Kameni A P, Couture-Tosi E, Saint-Girons I & Picardeau M (2002) *J Bacteriol* 184, 452–458
 - 22. Perkampus H-H (1992) *UV-VIS spectroscopy and its application*. Springer-Verlag Berlin Heidelberg, New York
 - 23. Pope V & Johnson R C (1991) J Clin Microbiol 29, 1548-1550
 - 24. Laemmli U K (1970) Nature 227, 680-685
 - 25. Gompertz B (1825) Philos Trans R Soc Lond 115, 513–585
 - 26. Maneewan S, Khedari J, Zeghmati B, Hirunlabh J & Eakburanawat J (2004), *Renew Energy* 29, 743–752

- 27. Bromley D B & Charon N W (1979) J Bacteriol 137, 1406-1412
- 28. Goldstein S F, Buttle K F & Charon N W (1996) J Bacteriol 178, 6539-6545
- 29. Nauman R K, Holt S C & Cox C D (1969) J Bacteriol 98, 264-280
- 30. Vile G F & Tyrrell R M (1995) Free Radical Biol Med 18, 721-730
- 5 31. Cadet J, Sage E & Douki T (2005) *Mutat Res* 571, 3–17
 - 32. Pfeifer G P, You Y H & Besaratinia A (2005) Mutat Res 571, 19-31
 - 33. Kramer G F & Ames B N (1987) J Bacteriol 169, 2259–2266
 - 34. Merwald H, Klosner G, Kokesch C, Der-Petrossian M, Honigsmann H & Trautinger F (2005) *J Photochem Photobiol B: Biol* 79, 197–207
- 10 35. Zhang X, Rosenstein B S, Wang Y, Lebwohl M & Wei H (1997) Free Radic Biol Med 23, 980–985
 - 36. Ramabhadran T V & Jagger J (1976) Proc Natl Acad Sci USA 73, 59-63
 - 37. Cheng F-C, Jen J-F & Tsai T-H (2002) *J Chromatogr B* 781, 481–496
 - 38. Nally JE, Timoney JF & Stevenson B (2001) Infect Immun 69, 400-404
- 39. Guerreiro H, Croda J, Flannery B, Mazel M, Matsunaga J, Reis M G, Levett P N, Ko AI & Haake D A (2001) *Infect Immun* 69, 4958–4968
 - 40. Zeilstra-Ryalls J, Fayet O & Georgopoulos C (1991) *Annu Rev Microbiol* 45, 301–325
 - 41. Stamm L V, Gherardini F C, Parrish E A & Moomaw C R (1991) *Infect Immun* 59, 1572-1575
 - 42. Cullen P A, Cordwell S J, Bulach D M, Haake D A & Adler B (2002) Infect Immun 70, 2311-2318
 - 43. Cullen P A, Haake D A, Bulach D M, Zuerner R L, Adler B (2003) *Infect Immun* 71, 2414-2421
- 25 44. Priya C G, Bhavani K, Rathinam S R & Muthukkaruppan V R (2003) *J Med Microbiol* 52, 667–673
 - 45. Fujishima A & Honda K (1972) *Nature* 238, 37–38.
 - 46. Ireland J C, Klostermann P, Rice E W&Clark R M (1993) *Appl Environ Microbiol* 59, 1668–1670.

40

Table 1—MAT reactivity of leptospiral samples after UVA exposure for various time intervals

No.	Exposure time	Dilution of reference antise				e antiserur	n tested	
		1:100	1:200	1:400	1:800	1:1600	1:3200	1:6400
1	0 min	4+	4+	3+	2+	1+	1+	-
2	5 min	3+	3+	2+	2+	1+	-	-
3	15 min	3+	3+	2+	2+	1+	-	-
4	30 min	3+	3+	2+	1+	1+	-	-
5	60 min	3+	3+	2+	2+	1+	-	
6	120 min	3+	3+	2+	2+	1+	-	
7	360 min	2+	2+	2+	1+	-		
8	1 day	2+	1+	1+	-			
9	2 days	2+	1+	-				
10	3 days	2+	1+	-				
11	4 days	2+	1+	-				
12	5 days	2+	1+	-				
13	6 days	2+	1+	-				
14	7 days	2+	1+	-				

4+, 3+, 2+, 1+ = variable degree of agglutination reactivity

Figure Captions.

Fig. 1—Side view schematic representation of the structure of *Leptospira*

5

Fig. 2—The growth curve of L. interrogans serovar Canicola. Relationship between Optical density (OD) values (at wavelength 400 nm) versus days of bacterial cultivation, 1, 2, 3, 4, 5, 6, and 7 days with EMJH liquid medium as a blank can be well fitted Gompertz function.

10

Fig. 3 a —Dark field micrographs of *L. interrogans* serovar Canicola exposed to UVA for different durations, 0 min, 30 min, 1 h, 6 h, 1 day, and 5 days. [Images were taken at the 7^{th} day of each experimental culture sample (diluted 1:10) with magnification 400x. Bars: 50 μ m]

15

20

Fig. 3 b: AFM micrographs of spiral shape using atomic force microscope (Seiko Instrument Inc., Japan) in dynamic mode with micro cantilever type: SI-DF20 K-A102001604, f = 135 kHz, spring constant 13 N/m (Seiko Instrument Inc., Japan). Scan area size was 2 x 2 μm^2 . Control sample unexposed to UVA; the leptospira had an approximate wavelength of 0.5 μ m (A), compared with 24 h UVA-exposed leptospira (B) with some cells having longer period than others.

Fig. 3 c: SEM micrographs of spiral shape taken using scanning electron microscope (Hitachi, Japan) with 15 kV [Magnification 6000v, Control sample unaversed to

(Hitachi, Japan) with 15 kV [Magnification 6000x. Control sample unexposed to UVA; the leptospira had a consistent wavelength (A) compared with 24 h UVA-exposed leptospira (B) with some cells having longer period than others]

30

Fig. 4—Dependence of the optical density $(OD_{400 \text{ nm}})$ of leptospira on exposure times [Exposure times (A) 0, 5, 15, 30, 45, 60, 120,180, 360, and 1440 min; and (B) 0, 1, 2, 3, 4, 5, 6, and 7 days. All samples were measured at 7^{th} day of cultivation and the experiment was repeated at 3 times]

30

35

Fig. 5—Dark field micrographs of agglutinated bacterial cells [The images were after reacting agglutinated bacterial cells with homologous antiserum (anti-canicola). (A) Micrograph showing complete agglutination of control or unexposed sample; and (B) Micrograph shows incomplete agglutination of 1-day exposure sample at 1:100 dilution, with magnification of 200x]

40

Fig. 6—Immunoblot of *L. interrogans* serovar Canicola antigen [Antigens were extracted from the cells on the 7th day of cultivation (Lane 1, control without UVA exposure); lanes 2-4, samples exposed to UVA for 2, 6 and 24 h respectively. The 21 kDa band disappeared after 24 h of exposure]

45

Fig. 7—SDS-PAGE analysis of the protein expression in leptospira [The gels were stained by Coommasie brilliant blue staining in presence of UVA for 2 h (lane 1), 6 h (lane 2), 24 h (lane 3), control sample (lane 4) and a standard molecular mass marker (lane 5). All samples exposed to the UVA radiation expressed the 76 kDa band significantly]

Figure Captions.

- Fig. 1 **Side-view schematic representation of the structure of** *Leptospira*Fig. 2 **The growth curve of** *L. interrogans* **serovar Canicola**. Relationship between Optical density (OD) values (at wavelength 400 nm) versus days of bacterial cultivation, 1, 2, 3, 4, 5, 6, and 7 days with EMJH liquid medium as a blank can be well fitted Gompertz function.
- Fig. 3 **Dark field micrographs of** *L. interrogans* **serovar Canicola**. 3(a): Dark field micrographs of *L. interrogans* serovar Canicola exposed to UVA for different durations, 0 min, 30 min, 1 h, 6 h, 1 day, and 5 days [Images were taken at the 7th day of each experimental culture sample (diluted 1:10) with magnification 400x. Bars: 50 µm]
- Fig. 3(b): AFM micrographs of spiral shape using atomic force microscope (Seiko instrument inc. Japan) in dynamic mode with micro cantilever type: SI-DF20 K-A102001604, f = 135kHz, spring constant 13 N/m (Seiko instrument inc. Japan). Scan area size was 2 x 2 μm². Control sample unexposed to UVA; the leptospira had an approximate wavelength of 0.5 μm (A) compared with 24 h UVA-exposed leptospira
 (B) with some cells having longer period than others.
 - Fig. 3(c): SEM micrographs of spiral shape taken using scanning electron microscope (Hitachi, Japan) with 15 kV [Magnification is 6000x. Control sample unexposed to UVA; the leptospira had a consistent wavelength (A) compared with 24 h UVA-exposed leptospira (B) with some cells having longer period than others]

25

30

35

40

- Fig. 4 **Dependence of the optical density (OD**_{400 nm}) **on exposure times**. (A) Relationship between optical density (OD_{400 nm}) of leptospira and various exposure times (0, 5, 15, 30, 45, 60, 120,180, 360, and 1440 min). (B) Relationship between optical density (OD_{400 nm}) of leptospira and various exposure times (0, 1, 2, 3, 4, 5, 6, and 7 days. All samples were measured at 7^{th} day of cultivation, and the experiment was repeated at three times.
- Fig. 5 **Dark field micrographs of agglutinated bacterial cells** The images are the dark field micrographs of agglutinated bacterial cells after reacting with homologous antiserum (anti-canicola). (A) Micrograph shows complete agglutination of control or unexposed sample. (B) Micrograph shows incomplete agglutination of 1day exposure sample at 1:100 dilution with magnification of 200x.
- Fig. 6 **Immunoblot of** *L. interrogans* **serovar Canicola antigen.** The antigens are extracted from the cells on the 7th day of cultivation (Lane 1, control without UVA exposure); lanes 2-4, samples exposed to UVA for 2, 6 and 24 h respectively. The 21 kDa band disappears after 24 h of exposure.
- Fig. 7 **SDS-PAGE** analysis of the protein expression in leptospira. The gels were stained by Coomasie brilliant blue staining in presence of UVA for 2 h (lane 1), 6 h (lane 2), 24 h (lane 3), control sample (lane 4) and a standard molecular mass marker (lane 5). All samples which were exposed to the UVA radiation were found to have expressed the 76-kDa band significantly.
- Table 1 MAT reactivity of leptospiral samples after UVA exposure at variable time.

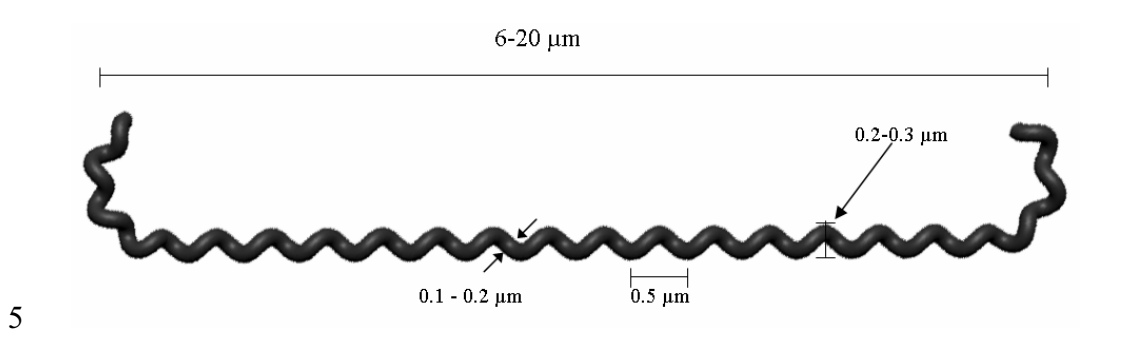


Fig. 1

10

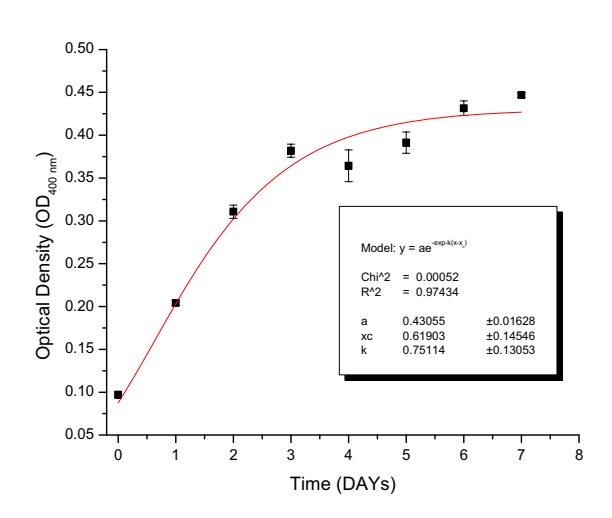
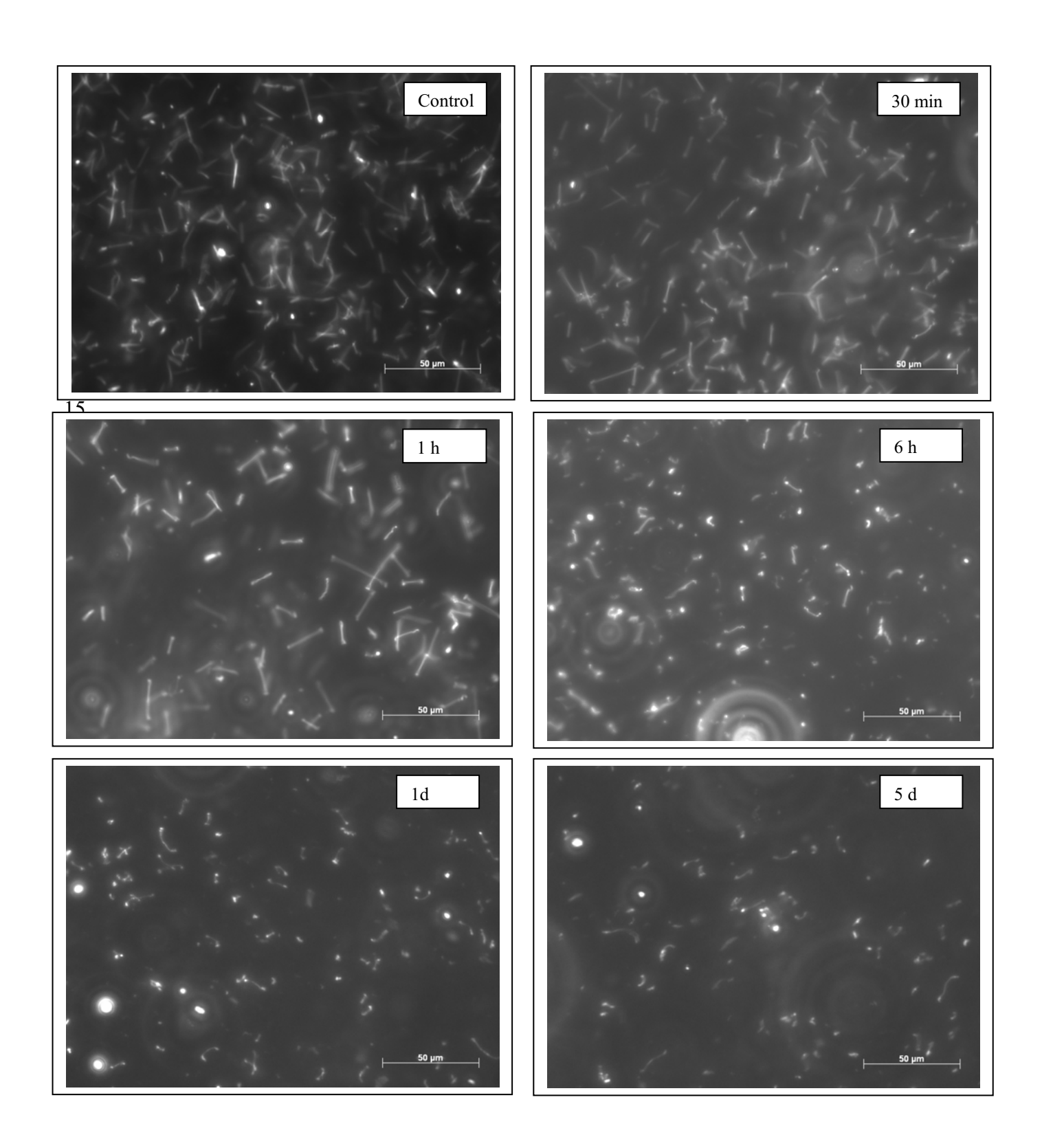


Fig. 2



35 **Fig.3a**

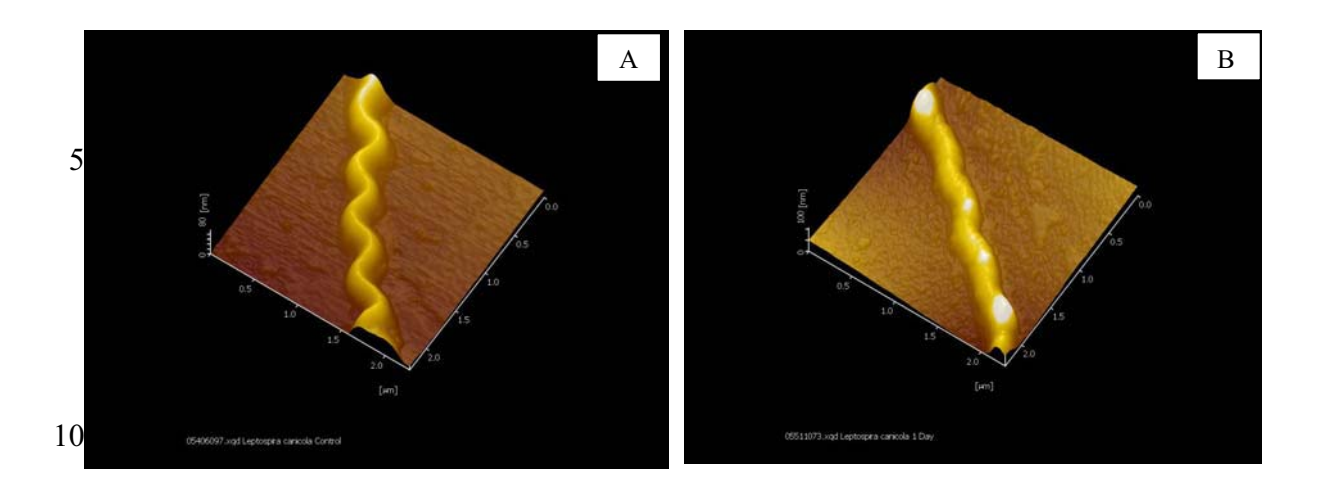


Fig. 3b

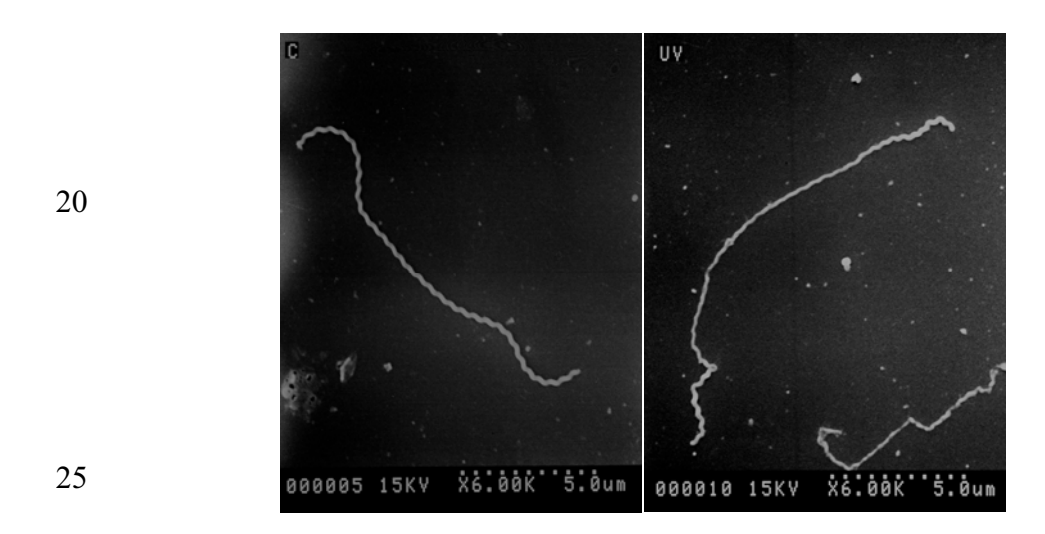


Fig. 3c

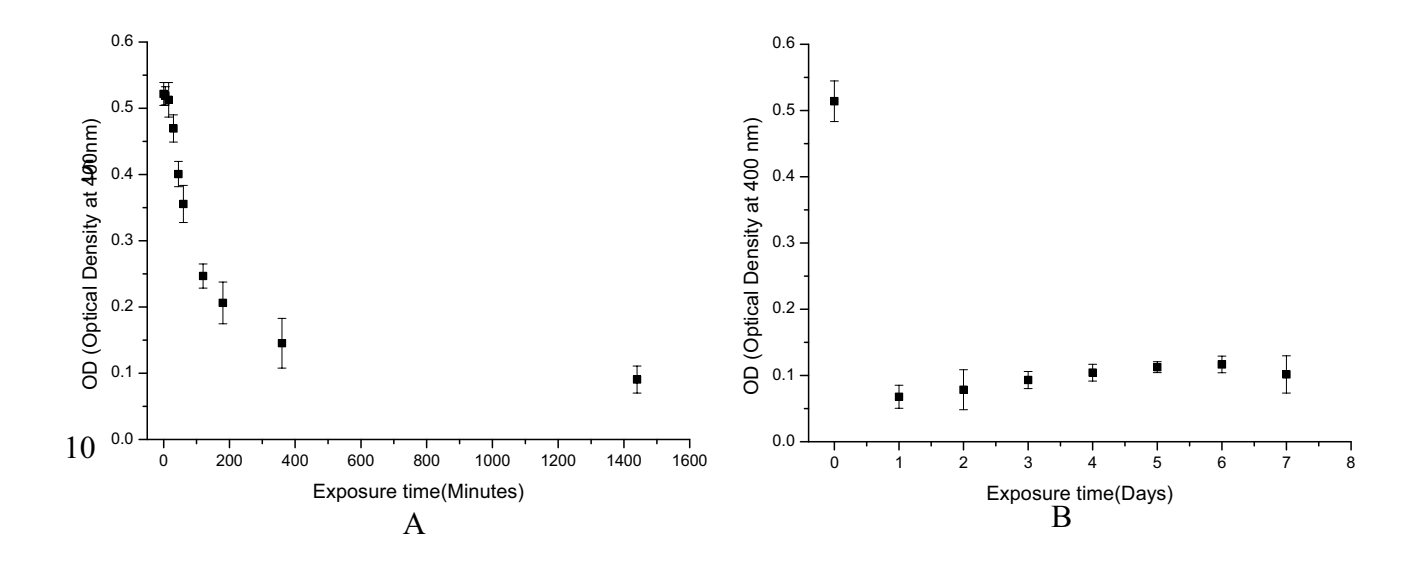


Fig. 4

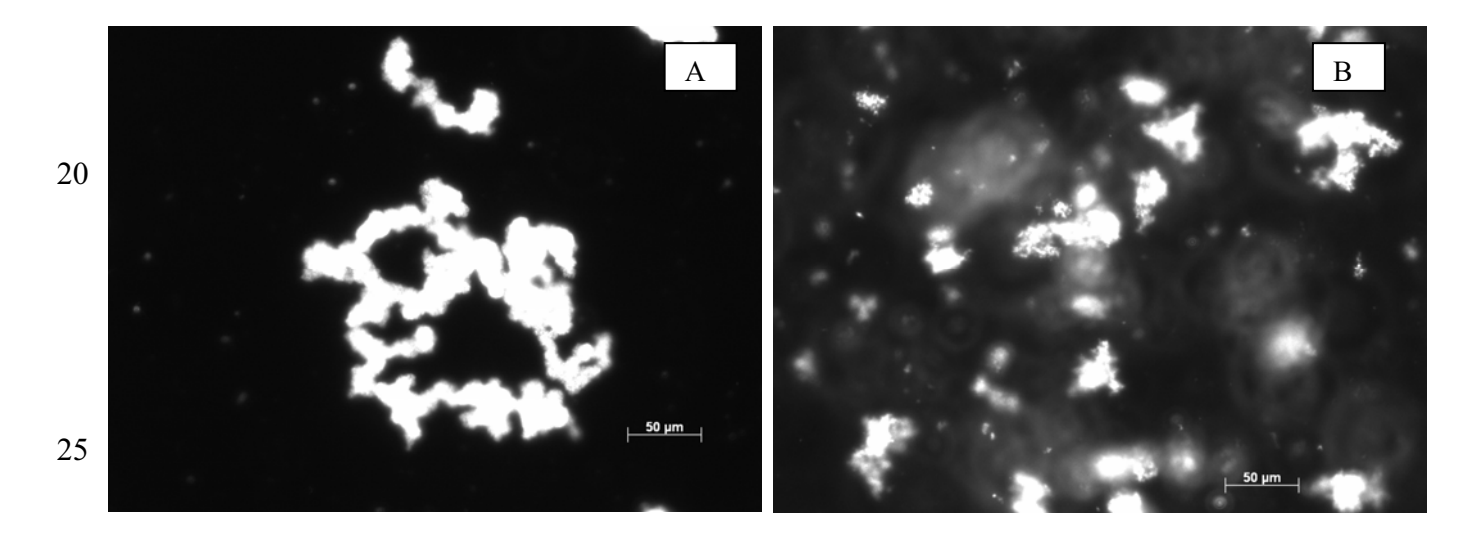


Fig. 5



Fig. 6

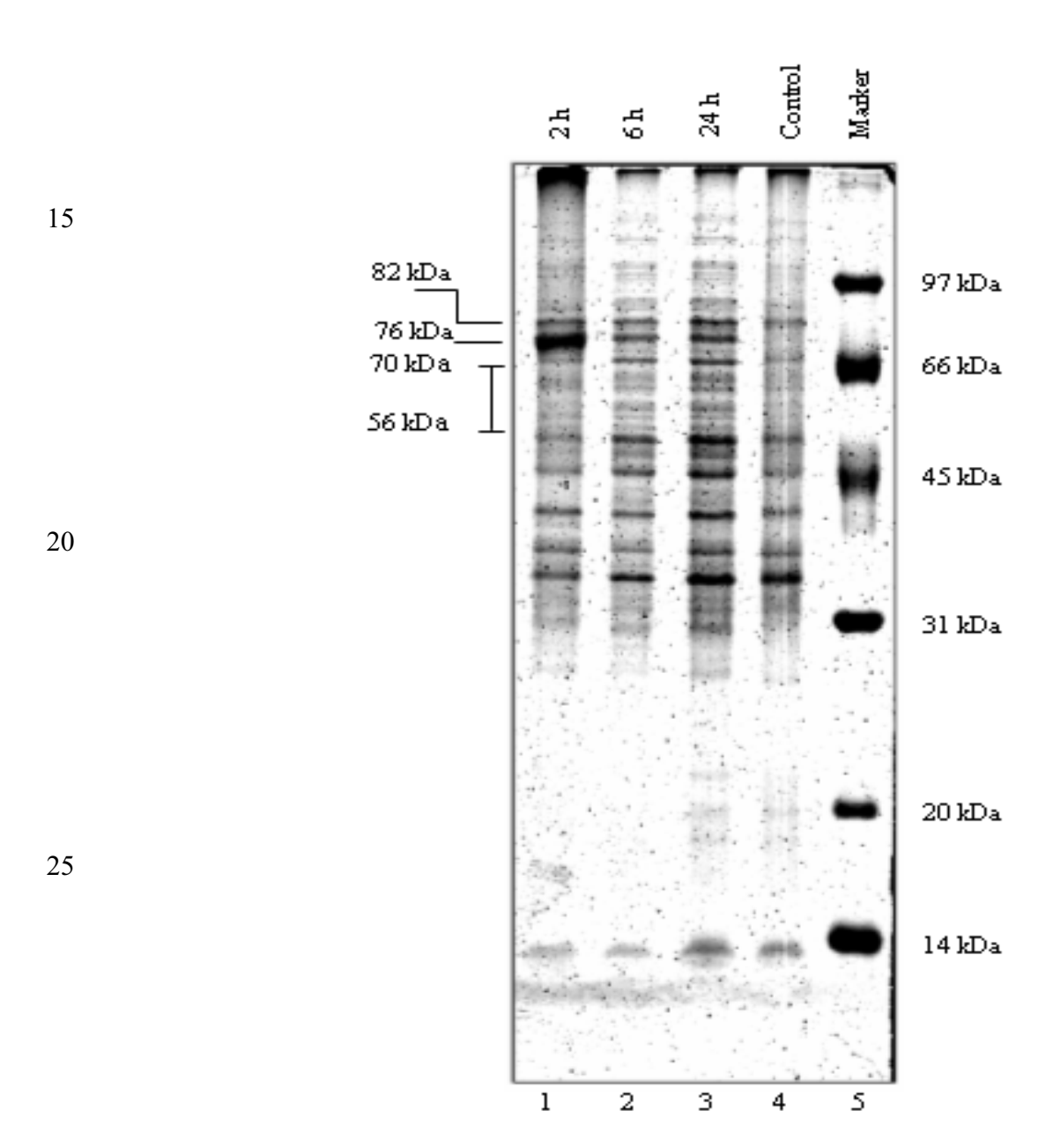


Fig. 7

Table 1 MAT reactivity of leptospiral samples after UVA exposure at variable time.

		Dilution of reference antiserum tested						
No.	Exposure time							
		1:100	1:200	1:400	1:800	1:1600	1:3200	1:6400
1	0 minutes	4+	4+	3+	2+	1+	1+	-
2	5 minutes	3+	3+	2+	2+	1+	-	-
3	15 minutes	3+	3+	2+	2+	1+	-	-
4	30 minutes	3+	3+	2+	1+	1+	-	-
5	60 minutes	3+	3+	2+	2+	1+	-	
6	120 minutes	3+	3+	2+	2+	1+	-	
7	360 minutes	2+	2+	2+	1+	-		
8	1 day	2+	1+	1+	-			
9	2 days	2+	1+	-				
10	3 days	2+	1+	-				
11	4 days	2+	1+	-				
12	5 days	2+	1+	-				
13	6 days	2+	1+	-				
14	7 days	2+	1+	-				

^{4+, 3+, 2+, 1+ =} variable degree of agglutination reactivity

Tracking MinD Proteins by the Single Particle Tracking Method

Somrit Unai^a, Paisan Kanthang^a, Udorn Junthon^a, Waipot Ngamsaad^a, Wannapong Triampo^{a,b,*},Charin Modchang^a, Chartchai Kritanai^c

5

- ^a R&D Group of Biological and Environmental Physics, Department of Physics, Faculty of Science, Mahidol University, Bangkok, Thailand
- ^b Center of Excellence for Vector and Vector-Borne Diseases, Faculty of Science, Mahidol University, Nakhonpathom, Thailand
- 10 ^c Institute of Molecular Biology, and Genetics, Mahidol University, Nakhonpathom, Thailand

Corresponding author

scwtr@mahidol.ac.th or wtriampo@yahoo.com

15 Department of Physics, Faculty of Science,

Mahidol University, Rama 6 Rd., Ratchatewee, Bangkok, 10400 Thailand

Phone: 662 441-9816 ext. 1131

Fax: 662 441-9322

Abstract

20

25

30

35

40

The dynamics of MinD protein has been recognized to play an important role in accurate positioning of the septum during cell division. In this work, the single particle tracking (SPT), was applied to quantitatively characterize the behavior of green protein fluorescence labeled MinD (GFP:MinD) in an Escherichia coli system, focusing on the position and motion of the maximum in the spatial distribution of MinD proteins.. The SPT data monitored from the dividing E. coli cells, 4.98±0.75 µm in length, has demonstrated a fast oscillation of the MinD protein between the two poles with average period of 54.63 ± 8.55 seconds. The results on the oscillating trajectory and velocity showed a trapping or localized behavior of MinD around the polar zone and the flight switching was observed at the pole-to-pole leading edge. From our analysis, we clearly found the dynamics to occur in two major instances, trapping events displayed in polar zones with average localization velocity of 0.2914±0.0584µm/s, and flight events displayed during pole switching with the average switching velocity of 2.95±0.31µm/s. The agreements between our findings and those from previous studies are discussed. These results have demonstrated the benefits of applying SPT to investigate the oscillation of targeted protein in both qualitative and quantitative aspects.

Keywords: Single Particle Tracking, E. coli, Cell division, Min proteins, MinD, protein oscillation

1. Introduction

5

10

15

20

25

30

35

40

45

In Escherichia coli and other rod-shaped bacteria, cell division depends on the precise placement of a division septum at the middle of the cell, a process initiated by the assembly of an equatorial ring (Z-ring) of the tubulin-like FtsZ GTPase on the cytoplasmic membrane (1, 2). The Z-ring assembly is spatially restricted to midcell by nucleoid occlusion (3, 4) and by the dynamics of Min system (5, 6). The nucleoid-free zones provide possible placement of Z-ring with three regions, two polar zones and a midcell zone, while the Min system prevents Z-ring assembly at the polar zone. The Min system consists of the MinC, MinD, and MinE expressed from the minB operon (5) which restricts separation to the desired potential division site at the midcell through the oscillatory cycle from pole to pole (reviewed in (7)). In vivo, MinC co-localizes and cooscillates with MinD (8, 9) which act together as a negative regulator of Z-ring assembly, and oscillatory dynamics depends on MinE (8-10). MinCD complex prevents the correct interaction of FtsA with the FtsZ ring in vivo (11), and MinC has been shown to inhibit FtsZ polymerization in vitro (8).

With regards to Min protein dynamics both in vitro and in silico, considerable number of experiments have been done. Computationally, several studies have been carried out with different reaction-diffusion models to explain these oscillations (12-17). It has also recently emerged that MinD forms helical filaments in living cells (18); and recent mathematical models (19, 21) have attempted to include this feature. The model by Drew et al. (19) includes polymer growth from nucleation sites at the ends of the cell. Both of these models use continuous partial differential equations. The model by Pavin et al. (21) differs in that it is a three-dimensional stochastic model, but it does not yield the observed large scale helical filaments. Incorporating stochastic feature introduced into Min modeling is nevertheless likely to be important for systems of this type (15, 21-24). Although almost all previous findings were able to provide both of great interest qualitative and quantitative predictions, only qualitative ones were verified. It was mainly because of the lack of quantitative experimental data. Therefore, more quantitative approach is considerably in need.

Experimentally, most works have focused on assembly and dynamics especially related to the spatial-temporal pattern formation and periods of MinCDE system. An excellent review is given by Lutkenhaus (25). In terms of technique based approaches, the majority of the works have used the fluorescent proteins with selectively labeled single proteins together with the high-resolution fluorescence imaging that is made possible by the new generation of bright-field and confocal microscopes (6, 8, 10, 18, 26-28). Of particular interest is the work by de Boer and co workers who studied the localization of MinD by monitoring membrane-associated protein of MinD in fixed E. coli cells. With the immunoelectron microscopy, anti-MinD antiserum and colloidal goldlabeled second antibody were used to reveal MinD associated with the cytoplasmic membrane (29). However, most, if not all, results are merely qualitatively good. The precise GFP-MinD or GFP-MinE data in terms of positions, velocity, trajectory, and so on, could be more improved. In fact, these data are still very rare, mainly because reliable position tracking, data processing and analysis software are still not very well known among the researchers in this particular field. To alternatively precisely track the positions in time-series of the region of interest (ROI) of Min proteins (provided by GFP-Min protein signals), the following conditions must be met; 1) the image capturing CCD must be fast enough, 2) the stages or samples must be stable enough to prevent the frame-shift at small length scale, 3) the noise or thermal fluctuation is not very large, and 4) the fluorescent signal consistently lasts long enough to retain reasonable data. Otherwise, the interpretation could easily be wrong or not reproducible. Though the subject of this Min protein dynamics is timely, more improved quantitative techniques are still in need. Indeed, based on above four mentioned criterion conditions, most current experimental works published so far on the Min system seem to satisfy these criteria. Here, SPT technique for quantitative study of the spatial-temporal pattern and the dynamics of MinD is one of our main focuses besides the MinD dynamics itself.

SPT is a computer-enhanced video microscopy that has been developed to measure not only the movement of single small molecules or particles, but also the trajectory of the molecule ensembles (30, 31). Mostly, it is used to track the motion of proteins or lipids on the cell surface, individual molecules or small clusters with a typical spatial resolution of tens of nanometers and a typical time resolution of tens of milliseconds. SPT have been used mostly in data analysis in order to classify the modes of motion (e.g. normal diffusion, anomalous diffusion, confined motion *etc.*) and to find the distribution of quantities characterizing the motion. As mentioned earlier, the data from SPT measurements generally constitute an important key for characterization of cell membrane. Hence, it is not only a probe of membrane microstructure, but can also contribute significantly to the study of reaction kinetics within the cell membrane. The SPT technique has been used in a large field of biophysical research such as in plasma and nuclear membrane studies (30), nuclear trafficking of viral genes (32), chromosome dynamics (33), and bacterial actins motion (34).

Motivated by the above mentioned considerations, this work has been devoted to the adaptation of this new technique for the quantitative study of Min protein dynamics. To the best of our knowledge, this is the first time ever that the SPT technique has been applied to this particular MinD dynamics problem. The focus is on the dynamics and localization of MinD protein pole-to-pole oscillations. As shall be seen later, our results not only will demonstrate how to apply SPT to MinD system, but also will confirm all previous qualitative results and could be used to provide, for example, characteristic timescale, reaction rate, diffusion coefficient, and so on. Hence, with regards to Min protein dynamics, not only the qualitative information can be obtained with this SPT technique, but much more direct quantitative information may be obtained as well. This allows us to more precisely and specifically answer the crucial questions associated with these phenomena. For example, how do particle ensembles move on the cell surface? How are the proteins assembled? Therefore, our results can potentially bridge the gap between the *in silico* and *in vitro* or *in vivo* experiments.

2. Materials and Methods **Bacterial strain and growth conditions**

E. coli RC1/pFX9 [$\Delta min/P_{lac}$ -gfp:: $\Delta minD$ $\Delta minE$] was kindly provided by Yu-Ling Shih (Department of Microbiology, University of Connecticut Health Health Center) (18). For examination of MinD labeled with green fluorescent proteins (GFP), a starter of RC1/pFx9 cells was grown in LB medium, 50 µg /ml ampilcillin, 25% of glucose at 37 °C and 250 rpm shaking overnight. Then 1% of the overnight culture was taken to grow in the new medium until the OD_{600nm} is approximately 0.4. The centrifugation was performed at 3,000 rpm for 15 minutes to collect the cells. Cells were then re-suspended in the same medium containing 0.1mM isopropyl-β-Dthiogalactopyranoside (IPTG) for protein induction. The cell culture was diluted with media before use.

15

10

5

Image acquisition

For fluorescence image sequences, the Zeiss Axioskop2 of fluorescence microscopy and A-plan, X100, 1.25 oil lenses were used with an InVivo software support in exposure times of 900 ms. A charge-coupled device (CCD) camera (CCD Revolution TM QEI Camera Monochrome) was attached to the video port of microscope to acquire images and movies in 1 frame/second. In our experimental preparation, the 5-7 µl of sample was dropped in a glass slide coated with 5 µl of Poly-L-lysine (0.1%) then covered by a cover slip at room temperature (25°C) before examination.

25

30

35

40

45

20

Image processing and SPT

The Single Particle Tracking (SPT) technique (30, 31) is used to follow the region of interest (ROI) which gives of the highest GFP:MinD concentration signal. This highest intensity is the representation of MinD ensemble in the cell. The data obtained from SPT measurements are supported by SpotTracker Java plugin of public domain ImageJ software (35). The SpotTracker is a robust and fast computational procedure to track fluorescent particles attached to the molecule of interest in time-lapse microscopy. The tracking process was performed in three steps as follows.

Firstly, the E. coli cell length in the raw fluorescence image sequence was rotated along to the major axis (x-axis) as shown in **Fig.1** (A-C). The goal of rotating the E. coli cell along to major axis is to make it simple and aligned for image analysis since the protein behavior is due to the MinD oscillations from pole to pole along the cell length.

Secondly, since the acquired image sequences, as shown in Fig.1 (A-C), are full of noise resulting from the thermal fluctuation and the fading of fluorescence signals (typically about 4-5 minutes after the beginning), subsequently at this stage the final image sequence is noisy. The corresponding intensity plot after reducing the noise is shown in Fig.1 (A'-C'). Realizing that this effect could reduce the accuracy of GFP:MinD ensemble positions collected from SpotTracker or lead to misinterpretation of the GFP:MinD phenomenon, the noisy images obtained must be further processed using a Gaussian filter with 2- pixel radius in order to reduce the effect of noise. It should be noted that if the pixel radius is too large, the positions of ROI are not accurate. Next, the low noise and signals were enhanced by using the rescaling option of SpotTracker plugin. One may feel somewhat of concern about the filters used. To us, this would be interesting research to improve the quality of the filtering procedure. As a consequence of the image enhancement process, the enhanced image, seen in Fig.1 (A"-C"), shows a better GFP signal than the raw fluorescence images in Fig.1 (A-C). The associated intensity signal is also shown in Fig.1 (A"-C"). As clearly seen, the consequence of the noise reduction is to make the region of high intensity more apparent.

Thirdly, the tracking procedure of ROI was performed using once again the SpotTracker plugin. With this tracking, it finally provides us with the time series data of the position of ROI of GFP:MinD system in text file ((x,y) coordinates) as shown in **Fig.1 (D-D"").** In this figure, the Red Cross sign indicates the ensemble positions at highest intensity signal. Finally, the positions of ensemble were analyzed by MATLAB software to calculate the physical quantities including velocity, period, and probability distribution. In fact, other dynamic quantities such as could also be calculated via this method. More details of this tracking in time algorithm can be found in (33).

3. Results and Discussions

20

25

30

35

5

10

15

Here we have applied SPT technique to experimentally and quantitatively investigate the pole-to-pole dynamics of the assembly dynamics of MinD proteins. With the combination of the SPT technique and image processing, we were able to demonstrate redistribution pattern of GFP:MinD (as mirror reflection of MinD proteins). Having focused on this dynamic behavior of MinD protein molecules, their moving positions are traced by the high intensity region as shown in **Fig.1** (A''-C'') and **Fig.1** (A'''-C'''). The SPT measurement provides the x and y coordinates of the center of ROI (for the visualization of ROI centers as shown in **Fig.1** (D-D'''')). The sequence of positions (x,y) at successive times can be used to determine the trajectory of GFP:MinD in x and y components as shown in **Fig.2** (B) and (C), respectively.

Having analyzed the high intensity regions in each frame of image sequences with enhanced filter shown on the right hand side of **Fig.2** (A), the results reveal the pole-to-pole oscillatory dynamics pattern between the polar zones. So far, at least it is qualitatively consistent with the previous findings with both experimental (8, 10, 18, 26-29, 36) and theoretical (12-16) methods. More importantly, using the extracted (x,y) allows us to precisely locate the positions of the MinD at a given time(see **Fig.2(D)**), portraying its trajectory.

From the obtained tracking positions, we can see that the assemblies of GFP-MinD molecules are mostly concentrated near the cytoplasmic membrane giving a horseshoe-like pattern. These results are well consistent with the previous reports of de Boer and co workers (29) that showed the localization of MinD in fixed *E. coli* cells. They employed anti-MinD antiserum and colloidal gold-labeled second antibody to study membrane-associated protein of MinD by using the immunoelectron microscopy to demonstrate that MinD is associated with the cytoplasmic membrane. In addition, our

results are in good agreement with those of fluorescent microscopy (10, 27, 28), which indicate that MinD localizes at the cytoplasmic membrane in the peripheral pattern.

Thanks to the quantitative data via SPT and consideration of the trajectory, we can precisely measure the average period of GFP:MinD ensemble that begins at the polar zone location and reverting to the same location (the trajectory cycle in **Fig.2(B)** and **Fig.3(A)**, or 3 peaks of velocity time evolution in **Fig.3(B)**). The measured period is 54.63 ± 8.55 seconds, averaging over 19 individual cells, with *E. coli* cell length of 4.98 ± 0.75 µm. Remarkably, our measured periods agree with those in previous reports (8, 10, 18, 26, 36) as shown in **Table 1**. However, it should be emphasized that either qualitative or semi-quantitative method were used to obtain all previous results. It is thus important to emphasize that having been able to obtain the quantitative data is one of the new distinct reward as a result of the SPT technique.

Owing to the quantitative data via SPT technique, the sequence of positions over each time interval reveals the trajectory and the velocities of proteins. Moreover, the ensemble GFP:MinD positions at all observable time allow us to analyze the assembly and pattern formation in the localization and distribution dynamics. These issues will be discussed in detail in the context of cluster dynamics and localization as follows.

Dynamics of GFP:MinD

5

10

15

20

25

30

35

40

45

The results from SPT technique provide us with information on position alterations and time sequences that can be used to analyze the GFP:MinD motion in two characteristics. (i) The trajectory reflects the positional behavior of cluster proteins as depicted in Fig.3 (A) and (A'). (ii) The velocity time evolution features movement behavior of cluster proteins as in Fig.3 (B) and (B'). Both results can indeed bring about the same information about the phenomenological characteristics of cluster protein motion. Typically, the characteristics of GFP:MinD protein dynamics can be classified according to the space and time scale of dynamic events into two types: *trapping event* and *flight event*. The trapping event mostly occurs at the polar zones, while the flight event takes place in between the trapping events in the space between the polar zones.

For the trapping events, It is quite evident from the data that the ensemble GFP:MinD trajectory positions change very little ($\leq 10\%$) during this state as evidently shown in Fig.3 (A) and (A'). Likewise, the velocities during those time intervals change very little during the time interval between peak to peak, as shown in Fig.3 (B) and (B'). This protein dynamic information implies that the MinD positions typically take relatively long time at the polar zones (~ 27 second). While the flight event takes considerably much lesser times (~ 2 -4 second). Therefore, the high concentrations of GFP:MinD are mostly found in the polar regions (see Fig.2(B)). We have learned from those previous studies that the dynamics of trapping events at polar zones are believed to correspond to the polar zone growth by the formation of MinD polymerization at cytoplasmic membrane (37, 38). It is also possible that MinD may interact with itself or other Min proteins or cytoplasmic components in a complicated manner not yet well

understood. One reaction diffusion model by Huang *et al.*(16) has proposed that this behavior is due to "cycling" of MinD in the polar zone whereby molecules repeatedly unbind and then quickly rebind.

For the flight event dynamics, as previously mentioned, the typical characteristics of the flight event are that the positions of the proteins quickly change from pole to opposite pole during a specific time interval. This dynamic behavior is clearly evidenced by the switching velocity, which corresponds to the peaks of each time interval mentioned earlier, as shown in Fig.3 (B) and (B'). Comparatively, the velocity associated with flight event is much higher than the velocity at the polar zone (~ 10 folds). During this state, as briefly mentioned in the introduction, when MinE in E-ring activates the ATPase activity of MinD:ATP molecules to undergo hydrolysis, it results in the release of the MinD:ADP, MinC, and MinE products from the membrane to the cytoplasm (7, 37-39). The MinE thus immediately sweeps MinD out of the midcell allowing Z-ring to form. The Z-ring assembly is spatially restricted to midcell by nucleoid occlusion (3, 4) and by the MinCDE system (5, 6). The first mechanism ensures that Z-rings form only in cellular space devoid of nucleoid mass, while the Min system prevents Z-ring assembly at the cell poles. This process is repeated when the MinD:ADP is converted to MinD:ATP in cytoplasm and continually diffuse to the opposite pole which gives rise the flight events and switching velocity.

GFP:MinD Localization

5

10

15

20

45

We have analyzed ensemble GFP:MinD localization through the histogram plots 25 shown in Fig.4(A-C) and position scattering plots shown in Fig.4(A'-C'). The data were collected during a 600 second time interval. Along the x-axis (or along the poles), it is clearly seen that MinD proteins mostly distribute and localize in the vicinity of the poles. This is spatially depicted by a two dimensional scattering plot. On the contrary, the region near the midcell has a lower concentration of MinD as previously reported (8-10, 30 26). To our knowledge, this is the first time that the time-averaged concentration of MinD (or division inhibitor), is experimentally and quantitatively revealed to be lowest at midcell as qualitatively known before. Accordingly, with this SPT technique, we are provided with the quantitative data of how local densities of MinD are distributed. This information would be of great value in predicting the specific site of localization and may be the reactions of MinD. Concerning the observed spatial inhomogeniety of MinD from 35 previous findings (15, 21-24), it was theorized that it is due to the helical movement during the Min protein polymerization. Therefore, when we perform a vertical section of E.coli, many SPT spots would be seen mostly on the top and at the bottom with somewhat constant intervals (data not shown). This phenomenon is expected to be clearly 40 seen when used the real time three dimensional image capturing and reconstructing techniques like confocal microscopy. Once again, on comparing these results with those from computational ones, good qualitative agreement was found

Fig.5 shows the distribution of ensemble GFP:MinD positions along the major axis. Blue dots represent the ensemble position data. From the least-square fitting procedure, the result of fitting gives a the symmetrical curve seen in this figure where the

red line represents the Gaussian function $y = y_0 + \frac{A}{w\sqrt{\pi/2}}e^{-2(x-x_c)^2/w^2}$ with $R^2 =$

0.93135. The middle position of distribution is equal to 2.29412 μ m for cell length ~ 5 μ m which is calculated from $x_{middle} = x_c - x_{min}$; $x_c = 2.54412 \pm 0.08606$ μ m and $x_{min} = 0.25$ μ m determined from the minimum point of MinD distribution position via GDF fitting and histogram, respectively. This graph quantitatively presents, for the first time ever, the distribution of MinD, though it was previously qualitatively reported (8-10, 26) that MinD proteins concentration is lowest at the midcell. Moreover, mathematical modeling and simulation results(12-19, 21) could also be validated and confirmed using our experimental results. It is surprising, however, that no report has shown the precise space-time plot and associated trajectories. It may be important to point out that the Gaussian function fitting may imply that the MinD dynamics is mediated by the concentration-gradient driven force of MinD or more precisely MinCDE system. It is possible that this graph may be used for determining where the midcell zone domain is or where the polar zone domain is. If so, it must be done with care and relevant biological considerations should be taken into account.

To summarize, with SPT technique we quantitatively found two major dynamic events, namely trapping events occurring in polar zones with average localization velocity of $0.2914\pm0.0584\mu\text{m/s}$ and flight events occurring during pole switching with the average switching velocity of $2.95\pm0.31\mu\text{m/s}$. The summary of the quantitative findings of localization and delocalization by using SPT is given in Table 2.

4. Concluding Remarks

25

30

35

40

5

10

15

20

The goal of this report was to propose the application of SPT to study MinD dynamics. In other words, it is to use computer-aided image analysis of fluorescence microscopy data. From our experimental results, acquisition of ensemble MinD position can be used to characterize and analyze the dynamic pattern formation, assembly, and localization. To our knowledge, this is the first time that it has been possible to observe, both qualitatively and quantitatively, the MinD dynamics. All results were qualitatively found to agree with previous experimental and theoretical results. Moreover, more precise quantitative information regarding MinD dynamics have also been obtained including specific positions, paths or trajectories, spatial distribution, pole-to-pole switching and localization, as well as periods. For example, our measured oscillation period is 54.63±8.55 seconds, which is a standard value of MinD period of oscillation for bacteria of this size and strain. It is reasonable to say that with SPT technique, the measurements performed are more accurate than by, say eye-observed measurement in 2D-image sequences. However, the accuracy of this SPT technique may be subject to environmental factors. A recent study shows that the period of MinD is dependent on the temperature in that the oscillation period rapidly decreases in proportion to increasing temperature (40).

An interesting characteristic of the time evolution dynamics is the trapping event that occurs between polar zones, a behavior that is still not well understood. With further improved SPT technique, especially applications in 3D, the information to be gained may reflect some mechanisms such as an obstruction of MinD by other mobile or immobile molecules or by other Min proteins, binding and obstruction by cellular components and so on. In terms of MinD localization, analyzing the ensemble positions using SPT technique, patterns of localization and distribution along the cell length were not only very well confirmed, but other quantitative information related to MinD ensemble positions were revealed as well.

It should be noted that *SPT* is for tracking the maximum of the distribution of particle ensemble, but not for single molecule. Here, they are likely tracking a constantly reorganizing accumulation of MinD proteins. Therefore, their velocity measurements are not actually single particle velocities either, and so are hard to compare with any microscopic quantities such as diffusion rates, etc.

For future application, we will use the same technique to investigate other Min protein types such as MinE or others. In addition, some important properties of the Min proteins such as the transport properties, energy landscape, fluctuation effects, rootmean-square distance dynamics, polymerization patterns, and so on are very interesting to be investigated. The data analysis of the distributions of periods and lengths of cells, to know how these quantities correlate, e.g. does period increase as length increases is on going process. Lastly, we believe that the SPT technique will be widely applied to the Min protein systems in the very near future like being used in other biological systems. Moreover, with improvement of the SPT technique, data acquisition and data analysis, this technique could become very well-accepted. The 3D, true to life results are of course what we strive for. Furthermore, by the combined use of SPT and the well known technique of fluorescent labeling or dyeing, it could be a considerably promising alternative over the other types of labeling, including the nanoparticle labeling approach.

Acknowledgements

We would like to greatly thank Prof. Lawrence Rothfield and Dr. Yu-Ling Shih (Department of Microbiology, University of Connecticut Health Health Center) for kindly providing $E.\ coli\ RC1/pFX9\ [\Delta min/P_{lac}-gfp::\Delta minD\ \Delta minE]$ for our use. Special thanks also go to Dr. Narin Nuttawut and Dr. Martin Howard for their fruitful discussions. The Development and Promotion of Science and Technology talents program to Waipot Ngamsaad. This work was supported by the National Center for Genetic Engineering and Biotechnology (BIOTEC), the Thailand Research Fund (TRF), the Third World Academy of Sciences (TWAS), and Institute of Science and Technology Development (ISTD).

References

5

15

20

25

- 1. Lutkenhaus, J., and S.G. Addinall. 1997. Bacterial cell division and the Z ring. *Annu. Rev. Biochem.* 66:93-116.
 - 2. Rothfield, L., S. Justice, and J. Garcia-Lara. 1999. Bacterial cell division. *Annu. Rev. Genet.* 33:423-48.
- 3. Woldringh, C. L., E. Mulder, P.G. Huls, and N. Vischer. 1991. Toporegulation of bacterial division according to the nucleoid occlusion model. *Res. Microbiol.* 142: 309-320.
 - 4. Yu, X. C., and W. Margolin. 1999. FtsZ ring clusters in min and partition mutants: role of both the Min system and the nucleoid in regulating FtsZ ring localization. *Mol. Microbiol.* 32:315-26.
 - 5. de Boer, P. A. J., R. E. Crossley, and L. I. Rothfield. 1989. A division inhibitor and a topological specificity factor coded for by the minicell locus determine proper placement of the division septum in *E. coli. Cell.* 56:641–649.
 - 6. Rothfield, L.I., Y.-L. Shih, and G. King. 2001. Polar explorers: membrane proteins that determine division site placement. *Cell*.106:13-6.
 - 7. Rothfield, L., A. Taghbalout, and Y.-L. Shih. 2005. Spatial control of bacterial division-site placement. *Nat. Rev. Microbiol.* 31:959-68.
- 8. Hu, Z., and J. Lutkenhaus. 1999. Topological regulation of cell division in *Escherichia coli* involves rapid pole to pole oscillation of the division inhibitor MinC under the control of MinD and MinE. *Mol. Microbiol.* 34:82-90.
 - 9. Raskin, D.M., and P.A. de Boer. 1999. MinDE-dependent pole-to-pole oscillation of division inhibitor MinC in *Escherichia coli*. *J. Bacteriol*. 181:6419-24.
 - 10. Raskin, D.M., and P.A. de Boer. 1999. Rapid pole-to-pole oscillation of a protein required for directing division to the middle of *Escherichia coli*. *Proc. Natl. Acad .Sci. USA*. 96:4971-6.
- 40 11. Justice, S. S., J. Garcia-Lara, and L. I. Rothfield. 2000. Cell division inhibitors SulA and MinC/MinD block septum formation at different steps in the assembly of the *Escherichia coli* division machinery. *Mol. Microbiol.* 37:410-423.
- Meinhardt, H., and P.A. de Boer. 2001. Pattern formation in *Escherichia coli*: a
 model for the pole-to-pole oscillations of Min proteins and the localization of the division site. *Proc. Natl. Acad. Sci. U S A.* 98:14202-7.

- 13. Howard, M., A.D. Rutenberg, and S. de Vet. 2001. Dynamics compartmentalization of bacteria: accurate division in *E. coli. Phys. Rev. Lett.* 87:278102-6.
- 14. Kruse, K. 2002. A dynamic model for determining the middle of *Escherichia coli*. *Biophys. J.* 82:618–27.
- 15. Howard, M., and A.D. Rutenberg. 2003. Pattern formation inside bacteria: fluctuations due to the low copy number of proteins. *Phys. Rev. Lett.* 90:128102-6.

15

20

25

30

35

- 16. Huang, K.C., Y. Meir, and N.S. Wingreen. 2003. Dynamic structures in *Escherichia coli*: spontaneous formation of MinE rings and MinD polar zones. *Proc. Natl. Acad. Sci. U S A*. 100:12724-8.
- 17. Modchang, C., P. Kanthang, W. Triampo, W. Ngamsaad, N. Nuttawut, and I.M. Tang. 2005. Modeling of the Dynamics Pole-to-pole Oscillations of the Min Proteins in Bacterial Cell Division: the Effect of an External Field. *J. Korean Phys. Soc.* 46:1031-36.
- 18. Shih, Y.-L., T. Le, and L. Rothfield. 2003. Division site selection in *Escherichia coli* involves dynamic redistribution of Min proteins within coiled structures that extend between the two cell poles. *Proc. Natl Acad. Sci. U S A.* 100:7865-70.
- 19. Drew, D.A., M.J. Osborn, and L.I. Rothfield. 2005. A polymerization-depolymerization model that accurately generates the self-sustained oscillatory system involved in bacterial division site placement. *Proc. Natl. Acad. Sci. U S A*. 102:6114-8.
 - 20. Meacci, G., and K. Kruse. 2005. Min-oscillations in Escherichia coli induced by interactions of membrane-bound proteins. *Phys. Biol.* 2:89-97.
- 21. Pavin, N., H.C. Paljetak, and V. Krstić. 2006. Min-protein oscillations in Escherichia coli with spontaneous formation of two-stranded filaments in a three-dimensional stochastic reaction-diffusion model. *Phys. Rev. E* 73:021904.
 - 22. Tostevin, F., and M. Howard. 2006. A stochastic model of Min oscillations in Escherichia coli and Min protein segregation during cell division. *Phys. Biol.* 3:1-12
 - 23. Fange, D., and J. Elf. 2006. Noise-induced Min phenotypes in *E. coli. PLoS Comput. Biol.* 2:e80.

- 24. Kerr, R.A., H. Levine, T.J. Sejnowski, and W.J. Rappel. 2006. Division accuracy in a stochastic model of Min oscillations in Escherichia coli. *Proc. Natl. Acad. Sci. U S A*. 103:347-52
- 5 25. Lutkenhaus, J. 2007. Assembly Dynamics of the Bacterial MinCDE System and Spatial Regulation of the Z Ring. *Annu. Rev. Biochem.* 76:14.1-14.24.

25

- 26. Hale, C.A., H. Meinhardt, and P.A. de Boer. 2001. Dynamics localization cycle of the cell division regulator MinE in *Escherichia coli*. *EMBO J.* 20:1563-72.
- 27. Rowland, S.L., X. Fu, M.A. Sayed, Y. Zhang, W.R. Cook, and L. Rothfield. 2000. Membrane redistribution of the Escherichia coli MinD protein induced by MinE. *J. Bacteriol* 182:613-9.
- 28. Szeto, T. H., S.L. Rowland, L.I. Rothfield, and G.F. King. 2002. Membrane localization of MinD is mediated by a C-terminal motif that is conserved across eubacteria, archaea, and chloroplasts. *Proc. Natl Acad. Sci. USA*. 99: 15693-98.
- 29. de Boer, P. A. J., R. E. Crossley, A. R. Hand, and L. I. Rothfield. 1991. The MinD protein is a membrane ATPase required for the correct placement of the *Escherichia coli* division site. *EMBO J.* 10:4371–4380.
 - 30. Saxton, M.J., and K. Jacobson. 1997. Single-particle tracking: applications to membrane dynamics. *Annu Rev Biophys Biomol Struct*. 26: 373-99.
 - 31. Qian, H., M. Scheetz, and E L. Elson. 1991. Single particle tracking. *Biophys. J.* 60: 910-21.
- 32. Babcock, H. P., C. Chen, and X. Zhuang. 2004. Using Single-Particle Tracking to Study Nuclear Trafficking of Viral Genes. *Biophys. J.* 87: 2749-58.
 - 33. Sage, D., F.R. Neumann, F. Hediger, S.M. Gasser, and M. Unser. 2005. Automatic tracking of individual fluorescence particles: application to the study of chromosome dynamics. *IEEE Trans Image Process.* 14:1372-83.
 - 34. Kim, S.Y., Z. Gitai, A. Kinkhabwala, L. Shapiro, and W.E. Moerner. 2006. Single molecules of the bacterial actin MreB undergo directed treadmilling motion in Caulobacter crescetus. *Proc Natl Acad Sci USA*. 103:10929-34.
- 40 35. SpotTracker: Single particle tracking over noisy images sequence. [Online]. Available: http://bigwww.epfl.ch/sage/soft/spottracker/ Web site of ImageJ: http://rsb.info.nih.gov/ij/
- 36. Szeto, J., N. F. Eng, S. Acharya, M. D. Rigdena, and J.A. Dillon. 2005. A conserved polar region in the cell division site determinant MinD is required for

- responding to MinE-induced oscillation but not for localization within coiled arrays. *Res. Microbiol.* 156:17–29.
- 37. Suefuji, K., R. Valluzzi, and D. RayChaudhuri. 2002. Dynamic assembly of MinD into filament bundles modulated by ATP, phospholipids, and MinE. *Proc. Natl Acad. Sci. USA* 99: 16776–81.
- 38. Hu, Z., E. P. Gogol, and J. Lutkenhaus. 2002. Dynamics assembly of MinD on phospholipid vesicles regulated by ATP and MinE. *Proc. Natl Acad. Sci. USA* 99: 6761–66.
 - 39. Hu, Z., and J. Lutkenhaus. 2001. Topological regulation of cell division in *E. coli*: spatiotemporal oscillation of MinD requires stimulation of its ATPase by MinE and phospholipid. *Mol. Cell* 7:1337-43.
 - 40. Touhami, A., M. Jericho, and A.D. Rutenberg. 2006. Temperature Dependence of MinD oscillation in *Escherichia coli*: Running Hot and Fast. *J. Bacteriol*. 188:7661-7.

20

15

30

35

40

Table legend

5

Table 1.

Oscillation cycle period(s) corresponding to each bacterial strain.

Table 2.

The physical properties of the ensemble GFP:MinD dynamics.

10

15 Tables

Strain/Plasmid	Genotype	Oscillation Cycle Period(s)	Reference
PB103(λDR122)	$wt(P_{lac}::gfp-minDE)$	~34	Raskin <i>et al.</i> (1999a)
PB103/pDR122	wt/P _{lac} ::gfp-minDE	~38	Raskin <i>et al.</i> (1999a) Hale <i>et al.</i> (2001)
PB114(λDR122)	$\Delta minCDE(P_{lac}::gfp-minDE)$	~40	Raskin <i>et al.</i> (1999a)
HL1/pDB213	Δ minDE/ P_{lac} ::gfp- minD, minE-bfp	~55	Hale et al. (2001)
pWM1255	P_{trc} :: gfp - $minD_{Ec}$, $minE_{Ec}$	~37	Ramirez-Arcos <i>et al.</i> (2002)
HL1/pFX40	ΔminDE_P _{lac} - yfp::minD minE	~60	Shih et al. (2003)

Table 1:

Properties	Mean Values	S.D.
Oscillation Period (s)	54.84	8.55
Switching Velocity (µm/s)	2.95	0.31
Localization Velocity (\(\mu m / s \)	0.2914	0.0584
Localization Time (s)	27.4194	4.9666

Table 2:

Figure legend

Figure 1.

Image processing and SpotTracking results for RC1 *E. coli* cell [min/P_{lac}-gfp::minD minE]. (A,B,C) shows raw fluorescence images at times 24s, 34s, and 44s. (A',B',C') shows intensity plot of fluorescence images corresponding to (A,B,C). (A'',B'',C'') shows fluorescence images of (A,B,C) after filtering with Gaussian blur and rescaling. (A''', B''', C''') shows intensity plot of images (A'', B'', C''). (D, D', D'', D''', D'''') shows fluorescence images after tracking with SpotTracker at times 24s, 44s, 64s, 84s, and 104s. The positions of ROI are indicated by red cross sign. (E) shows a DIC image (gray), cell length ~ 5 μm.

Figure 2.

15

20

25

The ensemble GFP:MinD oscillations from pole to pole at times 8s-279s with period of the approximately 45 seconds of period (A) The 2D image sequence of pole-to-pole MinD oscillations at each successive time for the rescaled and enhanced signal shown on the left and the right columns, respectively. Each fluorescence image represents the ensemble of GFP:MinD signal locating at polar zones. The time(s) labeled on the left side of column is the first time of GFP:MinD assembles after switching to new pole. (B) The results of SPT show the GFP signal time evolution trajectory of MinD oscillations on x(t). The red line represents the ensemble of GFP:MinD trajectory. (C) Spot projection on y(t) of GFP signal time evolution trajectory of MinD oscillations. (D) Time evolution plot of the position on x axis (blue line) and y axis (green line).

Figure 3.

The comparison of the time evolution dynamics between distance and velocity of *E. coli* cell for 600 seconds. (**A**) shows time evolution plot of the R ($R = \sqrt{(\Delta x)^2 + (\Delta y)^2}$) and (**A'**) shows subplot of R for the time interval 30-60 seconds. The distance-time evolution shows the oscillatory dynamics from pole to pole. (**B**) and (**B'**) show the velocity-time evolution throughout the time interval, and during a subinterval in time, respectively. The velocity-time evolution shows the switching velocity for each peak in (**B**) and localization velocity between peak to peak.

Figure 4.

The histogram and position scattering of GFP:MinD localization during 600 second time interval. (A), (B) and (C) are histograms that represent the localized frequency of GFP:MinD along x, y and R, respectively. (A'), (B') and (C') show the position scattering plotsof x-y, y-x and R-x, respectively.

Figure 5.

The distribution of ensemble GFP:MinD positions along the major axis. Blue dots represent the ensemble position data. The red line represents the fitted Gaussian function fitting $y = y_0 + \frac{A}{w\sqrt{\pi/2}} e^{-2(x-x_c)^2/w^2}$ with $R^2 = 0.93135$. The middle position of distribution is equal to 2.29412 μ m which is calculated from $x_{middle} = x_c - x_{min}$; $x_c = 2.54412 \pm 0.08606$ μ m and $x_{min} = 0.25$ μ m determined from the minimum point of MinD distribution position via GDF fitting and histogram, respectively.

15

20

25

30

35

40 Figures

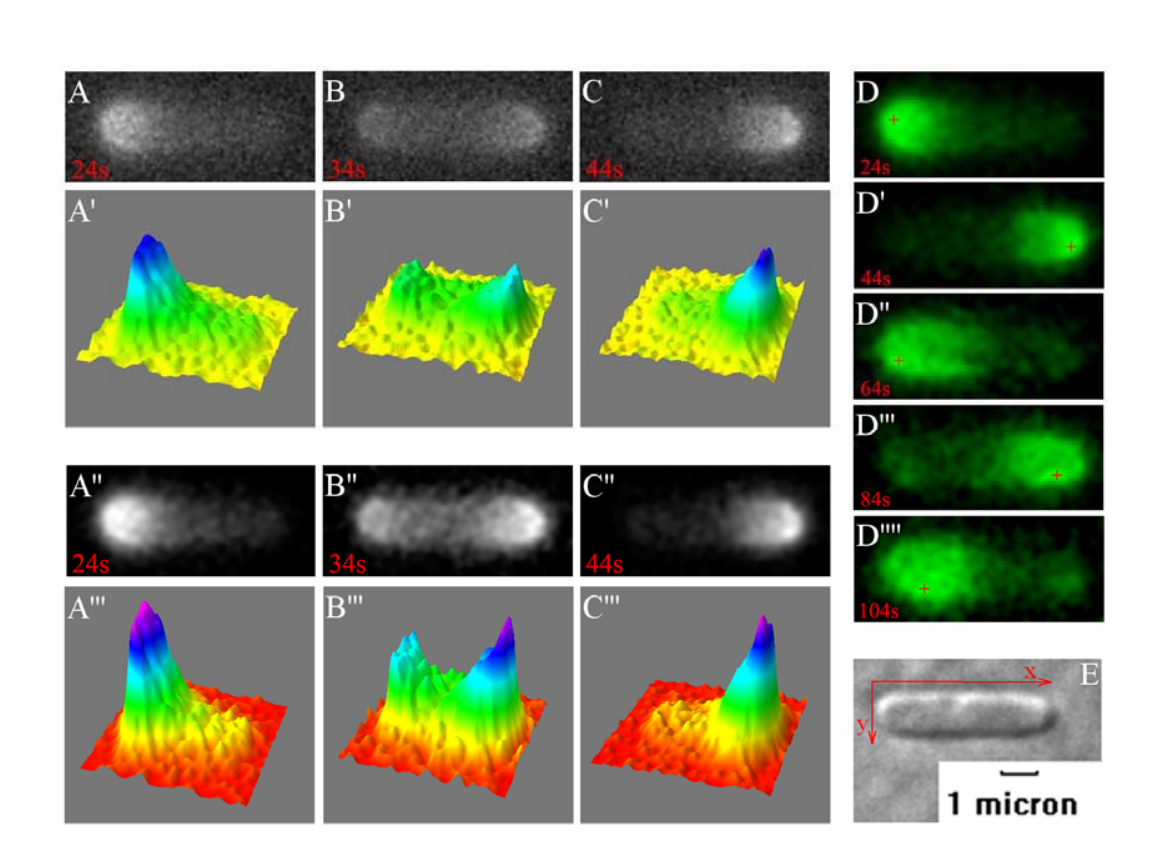


Figure 1:

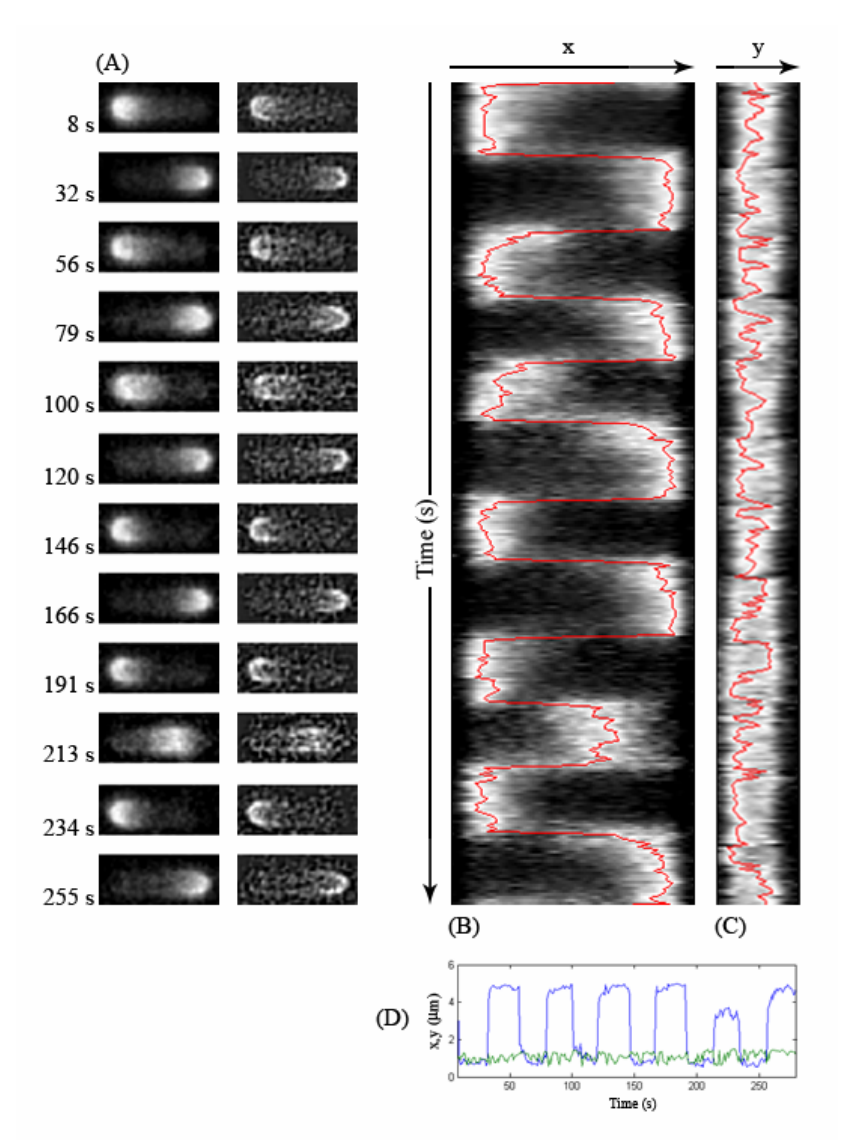


Figure 2:

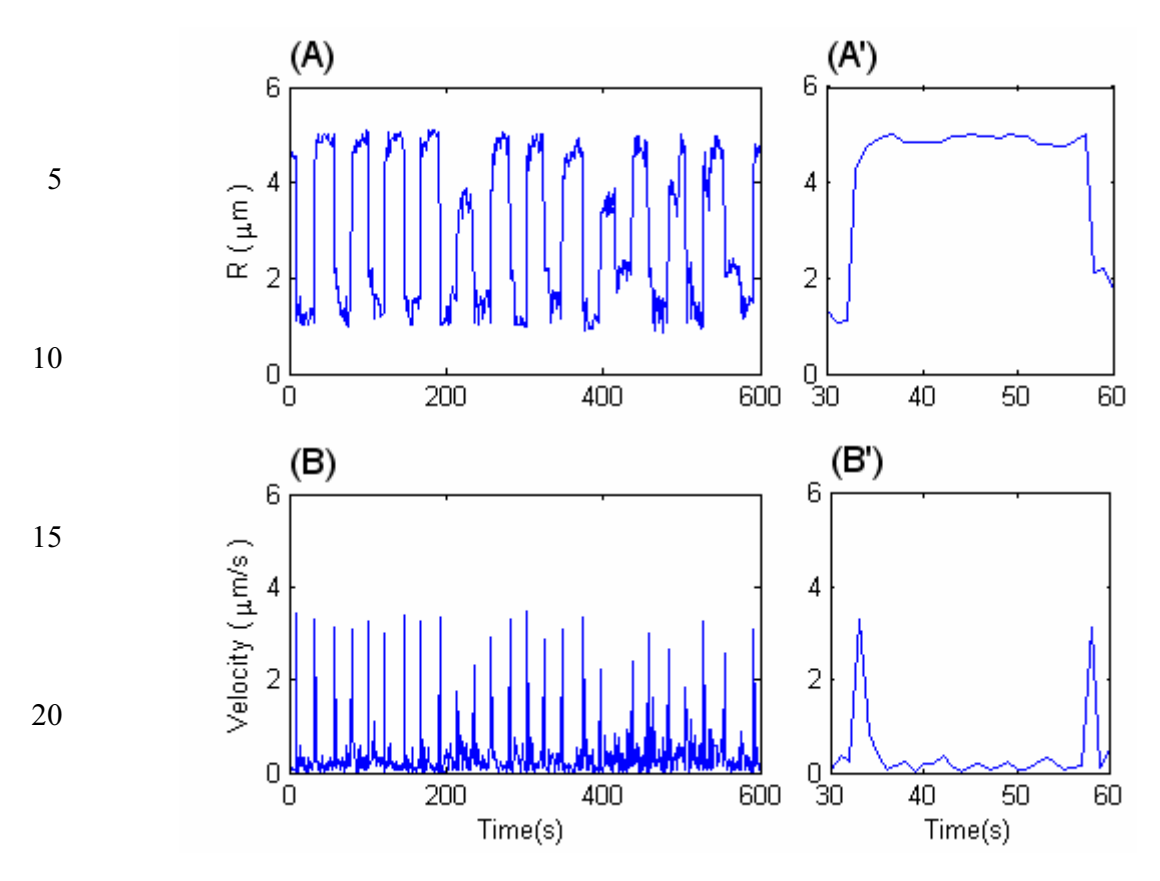


Figure 3: